iScience

CellPress
OPEN ACCESS

Article

Coordination between Cell Motility and Cell Cycle Progression in Keratinocyte Sheets via Cell-Cell Adhesion and Rac1

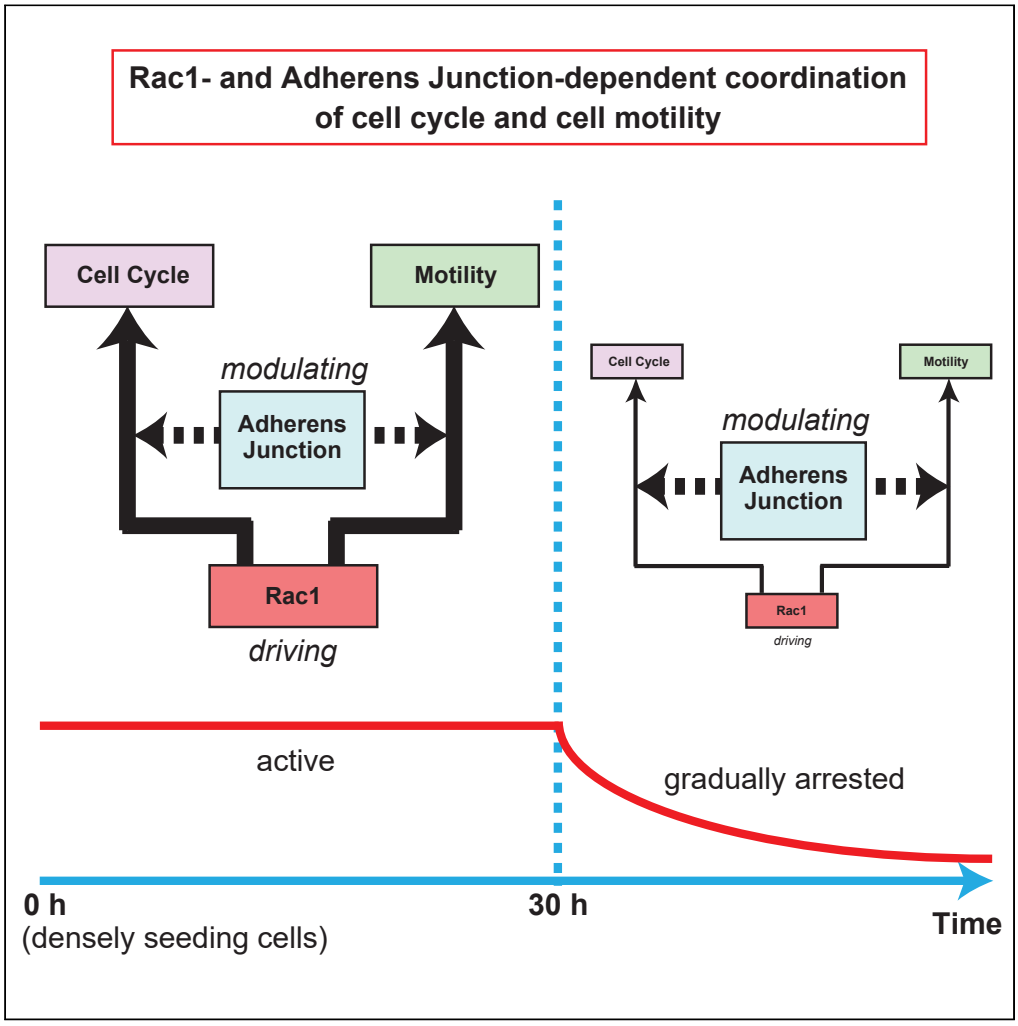

Hiroaki Hirata, Oleg Dobrokhotov, Masahiro Sokabe

hhirata@med.nagoya-u.ac.jp (H.H.)
msokabe@med.nagoya-u.ac.jp (M.S.)

HIGHLIGHTS

Cell motility and cell cycle progression in keratinocyte sheets are temporally coordinated

Rac1 promotes both cell motility and cell cycle progression in keratinocyte sheets

Arrest of cell motility and cell cycle is associated with Rac1 deactivation

Adherens junction is required for coordinating cell motility and cell cycle

Hirata et al., iScience *23*, 101729
November 20, 2020 © 2020 The Author(s).
https://doi.org/10.1016/j.isci.2020.101729

iScience

CellPress
OPEN ACCESS

Article

Coordination between Cell Motility and Cell Cycle Progression in Keratinocyte Sheets via Cell-Cell Adhesion and Rac1

Hiroaki Hirata,[1,2,*] Oleg Dobrokhotov,[1] and Masahiro Sokabe[1,*]

SUMMARY

Regulations of cell motility and proliferation are essential for epithelial development and homeostasis. However, it is not fully understood how these cellular activities are coordinated in epithelial collectives. In this study, we find that keratinocyte sheets exhibit time-dependent coordination of collective cell movement and cell cycle progression after seeding cells. Cell movement and cell cycle progression are coordinately promoted by Rac1 in the "early phase" (earlier than ~30 h after seeding cells), which is not abrogated by increasing the initial cell density to a saturated level. The Rac1 activity is gradually attenuated in the "late phase" (later than ~30 h after seeding cells), leading to arrests in cell motility and cell cycle. Intact adherens junctions are required for normal coordination between cell movement and cell cycle progression in both early and late phases. Our results unveil a novel basis for integrating motile and proliferative behaviors of epithelial collectives.

INTRODUCTION

Collective behaviors of cells are essential for development, regeneration, and homeostasis of tissues, wherein cells migrate, grow, proliferate, differentiate, and even die in a collective manner (Leevers and McNeill, 2005; Lecuit and Le Goff, 2007; Friedl and Gilmour, 2009; Aman and Piotrowski, 2010; Garcia-Hughes et al., 2015). In these processes, individual programs of collective behaviors are not operated independently, but need to be coordinated spatiotemporally. Strikingly, motility and proliferation of cell collectives are regulated in a correlated way depending on physiological and pathological situations. During embryogenesis, multiple rounds of cell proliferation expand tissues (Leevers and McNeill, 2005; Pan, 2007), while cells show active migration to achieve proper morphogenesis of tissues (Aman and Piotrowski, 2010). Once tissues have reached their optimal size and shape, cell motility and proliferation are arrested (Aman and Piotrowski, 2010; Hariharan, 2015). In adult tissues, even though most cells are largely quiescent in motility and proliferation, they regain abilities of collective migration and proliferation during wound repair and tissue regeneration (Shaw and Martin, 2009; Park et al., 2017). The highly motile and proliferative nature of cancer cells leads to their collective invasion and tumor growth (Friedl and Gilmour, 2009).

Recent advances in biophysical approaches have enabled to analyze the dynamic relationship between motility and proliferation of epithelial cell collectives. Confluent epithelial cells under spatial constraints are in a quiescent state, whereas removal of the constraints activates both cell motility and proliferation in a collective manner, leading to expansion of the epithelial sheet into the free space (Streichan et al., 2014; Uroz et al., 2018). In this process, dragging of the epithelial sheet by leader cells increases the area of individual follower cells in the sheet, which induces proliferation of follower cells by facilitating entry into S phase (Streichan et al., 2014; Uroz et al., 2018). By contrast, cell proliferation in an expanding epithelial sheet is arrested once the individual cell area becomes smaller than a critical value after filling up the available space or by subjecting the epithelial sheet to planar compression (Puliafito et al., 2012; Streichan et al., 2014). Based on these results, the individual cell area has been suggested as a critical parameter that determines proliferative behaviors of cells in an epithelial sheet (Puliafito et al., 2012; Aragona et al., 2013; Streichan et al., 2014; Uroz et al., 2018). On the other hand, serum stimulation of a confined, quiescent epithelial sheet can induce collective cell migration and proliferation without tissue expansion and an increase in the individual cell area (Lång et al., 2018), indicating that the increase in the individual cell area is not necessarily required to drive cell proliferation in migrating epithelial sheets. Thus, the mechanism

[1]Mechanobiology Laboratory, Nagoya University Graduate School of Medicine, Nagoya, Aichi 466-8550, Japan

[2]Lead Contact

*Correspondence: hhirata@med.nagoya-u.ac.jp (H.H.), msokabe@med.nagoya-u.ac.jp (M.S.)

https://doi.org/10.1016/j.isci.2020.101729

This is an open access article under the CC BY-NC-ND license (http://creativecommons.org/licenses/by-nc-nd/4.0/).

underlying coordinated regulation of cell motility and proliferation in epithelial collectives is not yet fully understood.

Collective cell migration in an epithelial sheet is driven by lamellipodia protrusion that is mediated by the small GTPase Rac1 (Fenteany et al., 2000; Tscharntke et al., 2007; Anon et al., 2012; Das et al., 2015). Furthermore, Rac1 is known to promote cell cycle progression and cell proliferation in various types of cells including epithelial cells (Olson et al., 1995; Moore et al., 1997; Liu et al., 2006; Molinie et al., 2019). While serum-induced collective migration and proliferation of epithelial cells depends on activation of the epidermal growth factor (EGF) receptor (Lång et al., 2018), EGF receptor activation leads to activation of Rac1 (Ridley et al., 1992; Kurokawa et al., 2004). Therefore, Rac1 is a potential candidate for regulating both cell motility and proliferation in an epithelial sheet (Park et al., 2017), even though its role in coordinating these two collective activities remains unresolved.

In this study, we find that monolayered keratinocytes (skin epithelial cells) exhibit time-dependent coordination of cell motility and cell cycle progression after seeding cells. Using this system, we reveal that Rac1 activity coordinately promotes cell motility and cell cycle progression in keratinocyte sheets and intact adherens junctions are required for the coordination of these cellular activities.

RESULTS

Time-Dependent Coordination of Cell Cycle Progression and Cell Motility in Keratinocyte Sheets after Seeding Cells

To monitor cell cycle progression and cell movement simultaneously in live cells, we introduced stably the Geminin-based Fucci fluorescent cell cycle probe, which is expressed in S, G_2, and M phases but degraded in G_1 and G_0 phases (Sakaue-Sawano et al., 2008), into human HaCaT keratinocytes. The HaCaT keratinocytes were densely seeded onto a collagen-coated substrate to fully cover the surface of the substrate with cells. The ratio of Geminin-positive cells first declined and then increased to peak around 30 h after seeding cells, which was followed by a decrease to a basal level by ~50 h after the seeding (Figures 1A and 1B; Video S1). The Geminin fluorescence observed in the initial stage (≤15 h after seeding cells) disappeared without cell division (Figure S1), indicating that the Geminin fluorescence in this time stage did not reflect the actual cell cycle and was therefore excluded from further analyses in this study. EdU incorporation also confirmed that S phase entry and progression were transiently increased around 30 h after seeding cells (Figure S2). Cell motility in the keratinocyte sheets was analyzed using particle image velocimetry (Figure S3). Local collective movements of cells were observed in the keratinocyte sheets (Figure 1A; Video S1). The cell motility was decreased later than ~30 h after seeding cells, reaching a basal level by ~50 h after the seeding (Figures 1A and 1C; Video S1). Thus, keratinocyte sheets show two temporal phases in terms of cell cycle progression and cell motility: the "early phase" (earlier than ~30 h after seeding cells) in which cell cycle progression and cell motility are promoted, and the "late phase" (later than ~30 h after seeding cells) in which cell cycle progression and cell motility are attenuated. Cell cycle progression and cell motility in sparse keratinocytes did not decline to basal levels later than ~30 h after seeding cells (Figure S4; Video S2), suggesting that attenuation of cell cycle progression and cell motility in keratinocyte sheets in the late phase represents confluence-dependent inhibition of cell proliferation and locomotion, termed contact inhibition (Mayor and Carmona-Fontaine, 2010; McClatchey and Yap, 2012; Puliafito et al., 2012; Hirata et al., 2017).

Following the increase in the ratio of Geminin-positive cells in the early phase, Geminin fluorescence in individual cells disappeared upon cell division (Figure S1). Thus, associated with a decrease in the ratio of Geminin-positive cells, the cell density in keratinocyte sheets was gradually increased in the late phase, reaching a plateau value ~1.5 times larger than the initial cell density (Figure 1D). This raised a possibility that the increase in the cell density might cause arrests in cell cycle and cell motility in the late phase. To address this point, we increased the initial cell density by 1.5 times (Figure 1E; Video S3) and examined cell cycle progression and cell motility. When we increased the initial cell density, the time-dependent increase in the cell density became less apparent, and the cell density level reached in the late time phase was not affected (Figures 1E and S5). Thus, it is suggested that there is a saturated, homeostatic cell density in keratinocyte sheets. The increase in the initial cell density reduced the extent of cell cycle progression and cell motility in the early phase (Figures 1F and 1G). However, these cellular activities in the early phase were not totally arrested under the high cell density condition; a transient increase in the ratio of Geminin-positive cells was still obvious (Figure 1F), and the average speed of cell movement at 30-h time point was

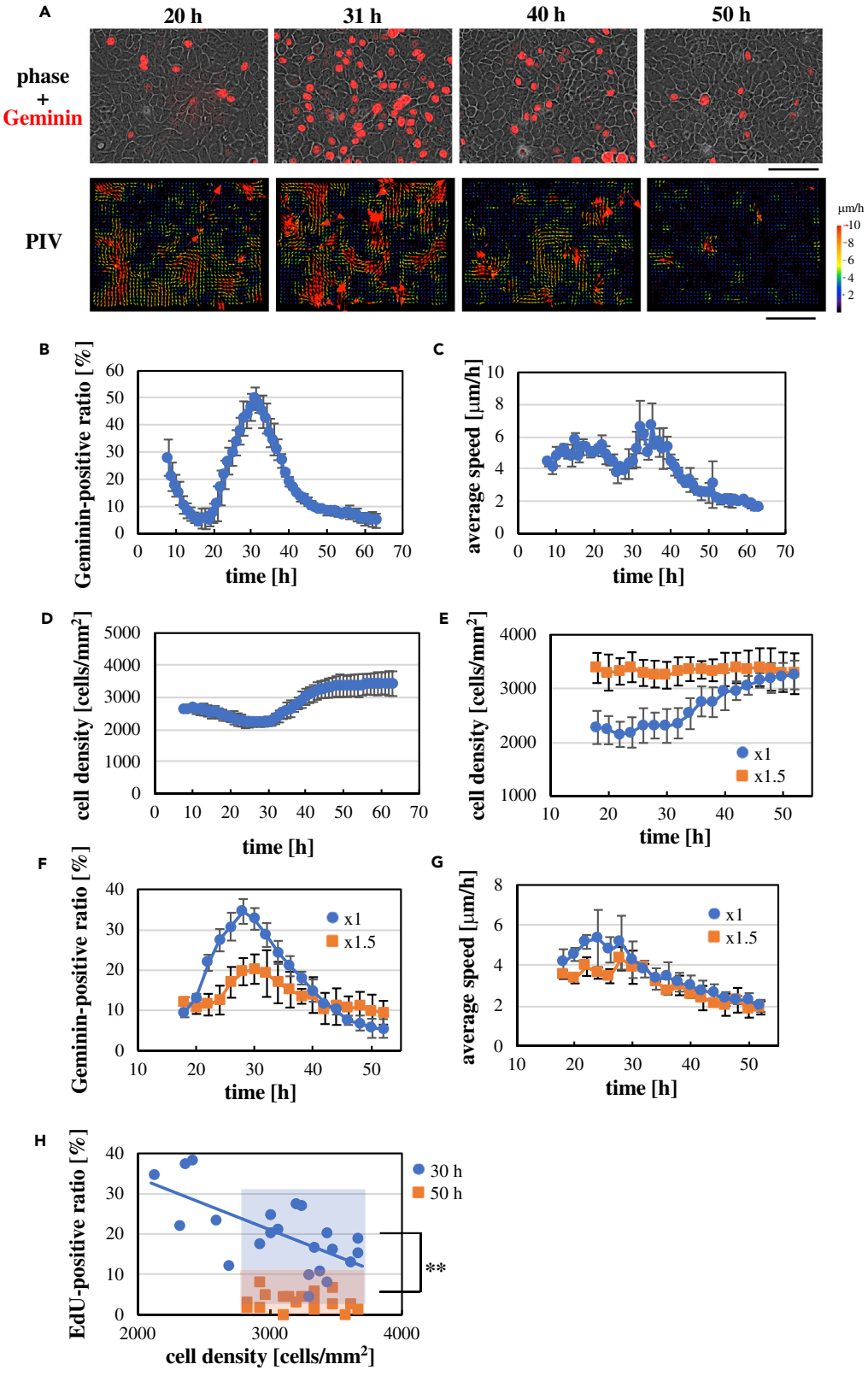
A
20 h
31 h
40 h
50 h
phase
+
Geminin
PIV
μm/h
10
8
6
4
2
B
Geminin-positive ratio [%]
time [h]
C
average speed [μm/h]
time [h]
D
cell density [cells/mm²]
time [h]
E
cell density [cells/mm²]
x1
x1.5
time [h]
F
Geminin-positive ratio [%]
x1
x1.5
time [h]
G
average speed [μm/h]
x1
x1.5
time [h]
H
EdU-positive ratio [%]
30 h
50 h
**
cell density [cells/mm²]

Figure 1. Time-dependent Changes in Cell Cycle Progression and Cell Motility in Keratinocyte Sheets

(A) Upper panels: Geminin-based Fucci fluorescence images (red) overlaid to phase contrast images of a HaCaT keratinocyte sheet at the indicated time points after seeding cells. Lower panels: velocity vector maps obtained by the particle image velocimetry analysis in the same keratinocyte sheet region at the same time points as those in upper panels. Scale bars, 100 μm.

(B–D) Time-dependent changes in the ratio of Geminin-positive cells against total cells (B), the average speed (C), and the cell density (D) in keratinocyte sheets after seeding cells. Each data point represents mean ± SD. n = 3 (>100 cells at each time point in each experiment in (B)).

(E–G) Time-dependent changes in the cell density (E), the ratio of Geminin-positive cells against total cells (F), and the average speed (G) in keratinocyte sheets after seeding different numbers of cells (20×10^5 cells for "×1," and 30×10^5 cells for "×1.5"). Each data point represents mean ± SD. n = 3 (>100 cells at each time point in each experiment in (F)).

(H) Relationship between nuclear incorporation of EdU and the cell density in keratinocyte sheets at 30- and 50-h time points after seeding cells. The ratio of EdU-positive cells and the local cell density were quantified in 22 regions (for "30 h") or 20 regions (for "50 h") of three keratinocyte sheets with different cell seeding densities, where each region contained >50 cells. The regression line of linear fitting for the "30-h" group is also shown. In the high-cell-density range (boxed regions colored in blue and orange), the ratio of EdU-positive cells was significantly higher at 30-h time point than that at 50-h time point (**$p < 0.01$; Student's two-tailed, unpaired t test). n = 16 (for "30 h") and 20 (for "50 h").

See also Figures S1–S7 and S16, and Videos S1, S2, S3, and S4.

significantly higher than that at 50-h time point (P = 0.031; Figure 1G). Consistently, when the ratio of EdU-positive cells was plotted against the cell density (Figure 1H) or the individual cell area (Figures S6B and S6C) in both early and late phases, keratinocyte sheets at 30-h time point showed a higher EdU-positive ratio than those at 50-h time point in the same high-cell-density range, even though the ratio of EdU-positive cells at 30-h time point decreased with increasing the cell density (Figures 1H and S6A). These results demonstrate that cell cycle and cell motility are not arrested in the early phase even at the saturated cell density. Apoptotic cell death promoted in the high-cell-density condition (Figure S7; Video S4) might contribute, at least in part, to maintaining the homeostatic cell density.

Time-Dependent Change of Rac1 Activity in Keratinocyte Sheets after Seeding Cells

Collective migration of epithelial cells during wound healing is driven by Rac1-dependent lamellipodia protrusion (Fenteany et al., 2000; Anon et al., 2012; Das et al., 2015). Hence, we next examined whether time-dependent changes in collective cell motility in keratinocyte sheets were associated with changes in Rac1 and lamellipodial activities. To visualize lamellipodial activity in individual cells, HaCaT cells expressing F-tractin-GFP were sparsely mixed with naive HaCaT cells, and they were densely seeded onto a collagen-coated substrate. Cells were actively protruding lamellipodia until ~30 h after seeding cells, whereas lamellipodial protrusion was gradually decreased later than ~30 h (Figures 2A and S8; Video S5), which was associated with gradual decline in cell motility in the late phase (Figures 1A and 1C). Consistently, when keratinocyte sheets were stained for the lamellipodia marker cortactin, the area of cortactin-positive lamellipodia was much smaller at 50-h time point compared with that at 30-h time point (Figures 2B, 2C, and S9).

Rac1 activity was measured in live keratinocyte sheets using the RaichuEV-Rac1 fluorescence resonance energy transfer (FRET) biosensor (Komatsu et al., 2011) that was stably introduced into HaCaT cells (Figure S10A). Intracellular localization of Rac1 was not affected by the cell cycle state or the time phase after seeding cells (Figures S10B–S10D). However, Rac1 activity gradually decreased later than ~30 h after seeding cells, reaching a basal level by 50-h time point (Figures 2D and 2E; Video S6). The PAK1-PBD-based pull-down assay also showed that the Rac1 activity at 50-h time point was lower than that at 30-h time point (Figure 2F). Hence, cell motility, lamellipodia protrusion, and Rac1 activity in keratinocyte sheets were high in the early phase, and all of them declined in the late phase.

Rac1 Coordinately Promotes Cell Cycle Progression and Cell Motility in Keratinocyte Sheets

Given a good correlation between cell motility and Rac1 activity in keratinocyte sheets, we asked whether Rac1 contributed to cell motility in the sheets. To address this, keratinocytes were seeded in the presence of the Rac1 inhibitor NSC 23766 (Gao et al., 2004). Although administration of the Rac1 inhibitor did not affect formation of intercellular adherens junctions (Figure S11), it reduced the Rac1 activity (Figure 3A) and abrogated formation of cortactin-positive lamellipodia (Figure 3B); instead, cortactin puncta containing F-actin were formed (Figure 3B). Associated with this, Rac1 inhibition lowered cell motility (Figure 3C; Videos S7 and S8). In addition, the transient increase in the ratio of Geminin-positive cells was eliminated upon Rac1 inhibition (Figure 3D; Videos S7 and S8). These results indicate that Rac1 activity is involved in

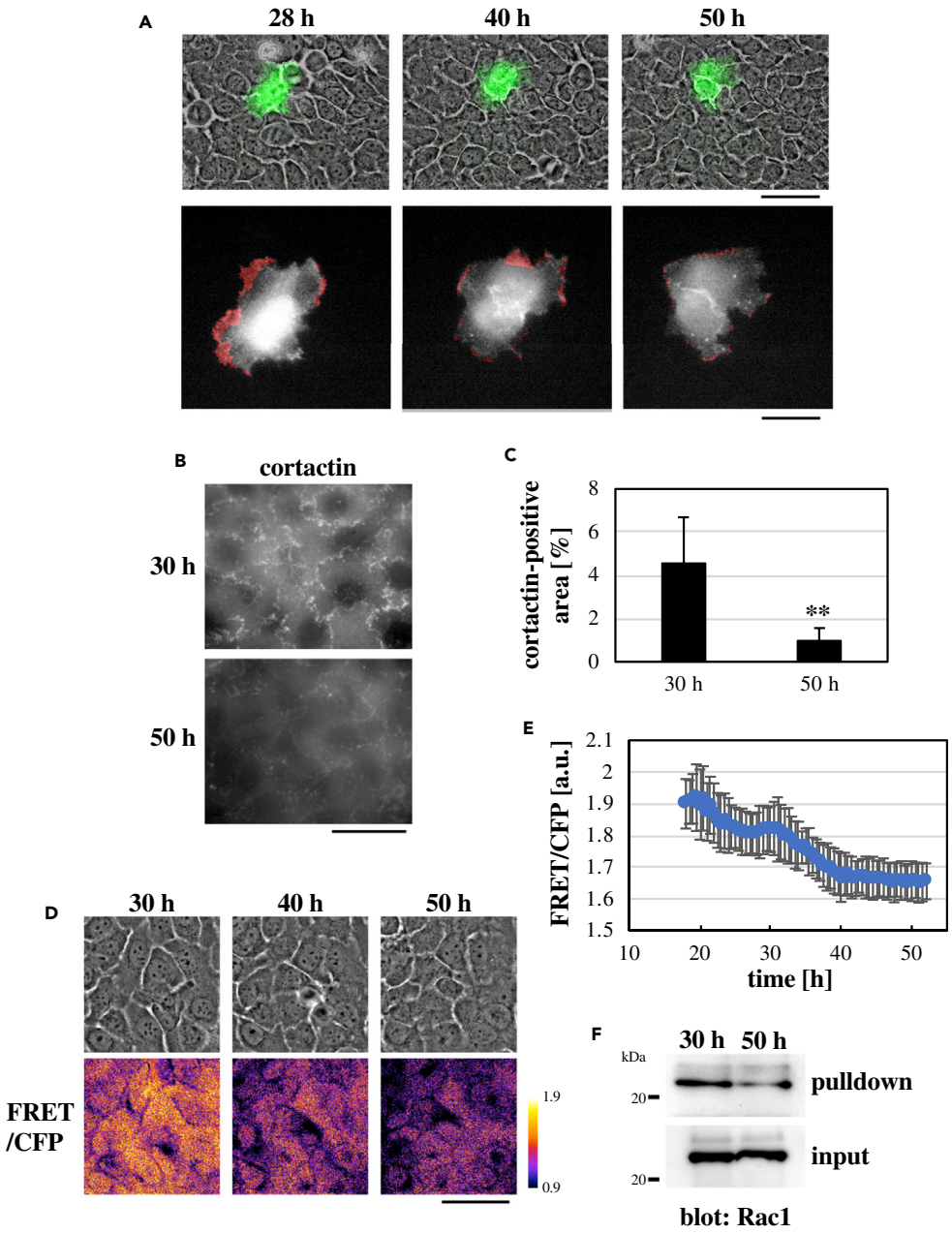

Figure 2. Time-Dependent Change in the Rac1 Activity in Keratinocyte Sheets

(A) F-tractin-GFP-expressing HaCaT cells were sparsely mixed with naive HaCaT cells. Upper panels: F-tractin-GFP images (green) overlaid to phase contrast images of a keratinocyte sheet at the indicated time points after seeding cells. Lower panels: magnified views (shown in gray scale) of the F-tractin-GFP-expressing HaCaT cell in the upper panels. Regions of the cell that have been extended in the last 30 min before the indicated time points are shown in red. Scale bars: 100 μm for upper panels and 50 μm for lower panels.

(B) Immunofluorescence images of cortactin in keratinocyte sheets at the indicated time points after seeding cells. Scale bar, 30 μm.

(C) Percentages of cortactin-positive lamellipodia regions against the total area of the view field at the indicated time points after seeding cells. Each bar represents mean ± SD. n = 10. **$p < 0.01$ (Student's two-tailed, unpaired t test).

(D) Phase contrast (top panels) and FRET/CFP ratio (bottom panels) images of a RaichuEV-Rac-expressing keratinocyte sheet at the indicated time points after seeding cells. Scale bar, 50 μm.

(E) Time-dependent change in the FRET/CFP ratio in RaichuEV-Rac-expressing keratinocyte sheets after seeding cells. Each data point represents mean ± SD. n = 3.

Figure 2. *Continued*
(F) Lysates of keratinocyte sheets at the indicated time points after seeding cells were subjected to the PAK1-PBD-based pull-down assay for active Rac1.
See also Figures S8–S10, and Videos S5 and S6.

promoting not only cell motility but also cell cycle progression in keratinocyte sheets. When the Geminin-positive cell ratio was plotted against the cell movement speed at each time point throughout the observation period for control and Rac1-inhibited conditions, it was shown that cell cycle progression and cell movement were coordinately attenuated by Rac1 inhibition (Figure 3E), demonstrating the crucial role of Rac1 in coordinately promoting cell cycle progression and cell motility. By contrast, spatial autocorrelation of the cell movement direction in a keratinocyte sheet was not affected by Rac1 inhibition (Figure S12), suggesting that collectiveness of cell movement in keratinocyte sheets does not depend on the Rac1 activity. After cell motility and cell cycle progression declined to basal levels (i.e., later than ~50 h after seeding cells), Rac1 inhibition did not further reduce these cellular activities (Figures 3C and 3D), which was consistent with the minimal activity of Rac1 in this time stage (Figures 2D and 2E).

Inhibition of Rac1 decreased the population of cells that were in S, G_2, and M phases (i.e., Geminin-positive) (Figure 3D), as well as the number of division events in each cell during the observation period (see Figure 6F). By contrast, for cells that entered S phase, duration of S to M phases (i.e., from appearance of the Geminin signal to cell division) was not altered upon Rac1 inhibition (Figure 3F). These results suggest that Rac1 inhibition does not affect progression of S, G_2, and M phases, but reduces the probability of S phase entry in keratinocyte sheets.

Intact Cell-Cell Adhesion Is Required for Rac1-Mediated Coordination of Cell Cycle Progression and Cell Motility

Cadherin-mediated cell-cell adhesion (adherens junction) is reportedly crucial for collective cell behaviors in epithelial sheets (Ng et al., 2012; Cai et al., 2014; Vedula et al., 2014). Cells in keratinocyte sheets developed punctate adherens junctions in their apical regions and circumferential adherens junctions in their middle regions (Figure S13). Thus, we examined whether the adherens junction was involved in coordination between cell cycle progression and cell motility in keratinocyte sheets. To this end, we stably depleted expression of the adherens junction component α-catenin in HaCaT keratinocytes (Figure 4A), which would destabilize adherens junctions (Vedula et al., 2014). In line with this expectation, α-catenin depletion in keratinocyte sheets caused formation of intercellular gaps at apical portions of cells, even though the cells remained in contact each other at their basal portions (Figure 4B). Cell motility was largely enhanced by α-catenin depletion in the early phase, but movement of α-catenin-depleted cells was decreased in the late phase to a basal level similar to that of control cells (Figure 4C; Videos S9 and S10). Depletion of α-catenin did not alter the activity of Rac1 (Figure S14), suggesting that enhancement of cell motility upon α-catenin depletion in the early phase was not mediated by an increase in the Rac1 activity. One may consider that formation of intercellular gaps upon α-catenin depletion (Figure 4B) provides spaces for cells to move; however, this scenario is unlikely, because increasing the initial cell density by 1.5 times to further pack cells did not reduce motility of α-catenin-depleted cells, which was in marked contrast to the case of control cells (Figure S15; see also Figure 1G). Spatial autocorrelation of the cell movement direction decayed more steeply (i.e., with a larger decay constant) in α-catenin-depleted keratinocyte sheets than in control ones (Figure S12), indicating that collectiveness of cell movement in keratinocyte sheets depends on α-catenin expression. On the other hand, the ratio of Geminin-positive cells was not affected by α-catenin depletion in the early phase, but its decline in the late phase was diminished in α-catenin-depleted cells (Figure 4D; Videos S9 and S10). This led to a monotonic increase in the density of α-catenin-depleted cells in the late phase (Figure 4E). Thus, expression of α-catenin influences cell cycle progression and cell motility differentially; α-catenin expression attenuates cell cycle progression only in the late phase, and reduces cell motility preferentially in the early phase. Accordingly, plots of the Geminin-positive cell ratio against the cell movement speed at each time point showed that correlation of these two parameters became less obvious upon depletion of α-catenin (Figure 4F). These results suggest that α-catenin-dependent intact adherens junction is involved in coordinated regulation of cell cycle progression and cell motility in keratinocyte sheets.

To further examine the effect for perturbation of adherens junctions, α-catenin was overexpressed in HaCaT keratinocytes. Compared with introduction of GFP only, introduction of GFP-tagged α-catenin (Figures S16A and S16B) decreased the ratio of Geminin-positive cells in keratinocyte sheets (Figure S16C). On the other hand,

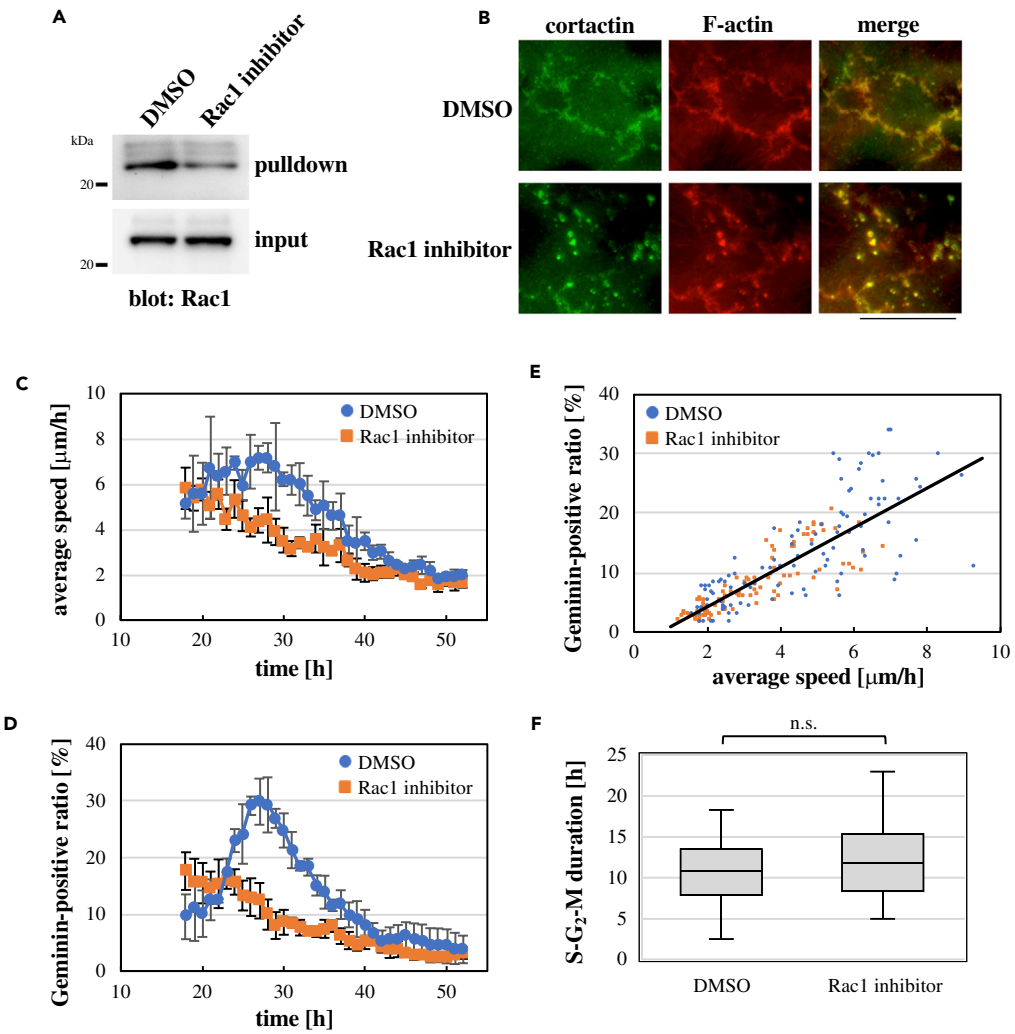

Figure 3. Rac1 Coordinately Promotes Cell Cycle Progression and Cell Motility in Keratinocyte Sheets

(A) Lysates of keratinocyte sheets grown for 30 h after seeding cells in the presence of DMSO (control) or the Rac1 inhibitor (20 μM NSC23766) were subjected to the PAK1-PBD-based pull-down assay for active Rac1.

(B) Immunofluorescence images of cortactin and F-actin in keratinocyte sheets at 30 h after seeding cells in the presence of DMSO (control) or the Rac1 inhibitor (20 μM NSC23766). Merged images are also shown. Scale bar, 30 μm.

(C and D) Time-dependent changes in the average speed (B) and the ratio of Geminin-positive cells against total cells (C) in keratinocyte sheets after seeding cells in the presence of DMSO (control) or the Rac1 inhibitor (20 μM NSC23766). Each data point represents mean ± SD. n = 3 (>100 cells at each time point in each experiment in (D)).

(E) The ratio of Geminin-positive cells was plotted against the average speed at each time point throughout observation under control (DMSO) and Rac1-inhibited (20 μM NSC23766) conditions. Data from three independent experiments were combined for each condition. The regression line of linear fitting is shown.

(F) Duration of S to M phases (i.e., from appearance of the Geminin signal to cell division) in individual cells within keratinocyte sheets under control (DMSO) and Rac1-inhibited (20 μM NSC23766) conditions. n = 36. n.s., no significant difference (Student's two-tailed, unpaired t test).

See also Figures S11 and S12, and Videos S7 and S8.

overexpression of α-catenin-GFP increased the average speed of cell movement in the early phase (Figure S16D). As both depletion (Figure 4C) and overexpression (Figure S16D) of α-catenin resulted in promotion of cell movement, an optimal level of α-catenin expression would be essential for normal cell motility in keratinocyte sheets. Thus, overexpression of α-catenin differentially altered the Geminin-positive cell ratio and the cell movement speed (Figure S16E), which again suggested that α-catenin-mediated adherens junction is crucial for the normal coordination of cell cycle progression and cell motility in keratinocyte sheets.

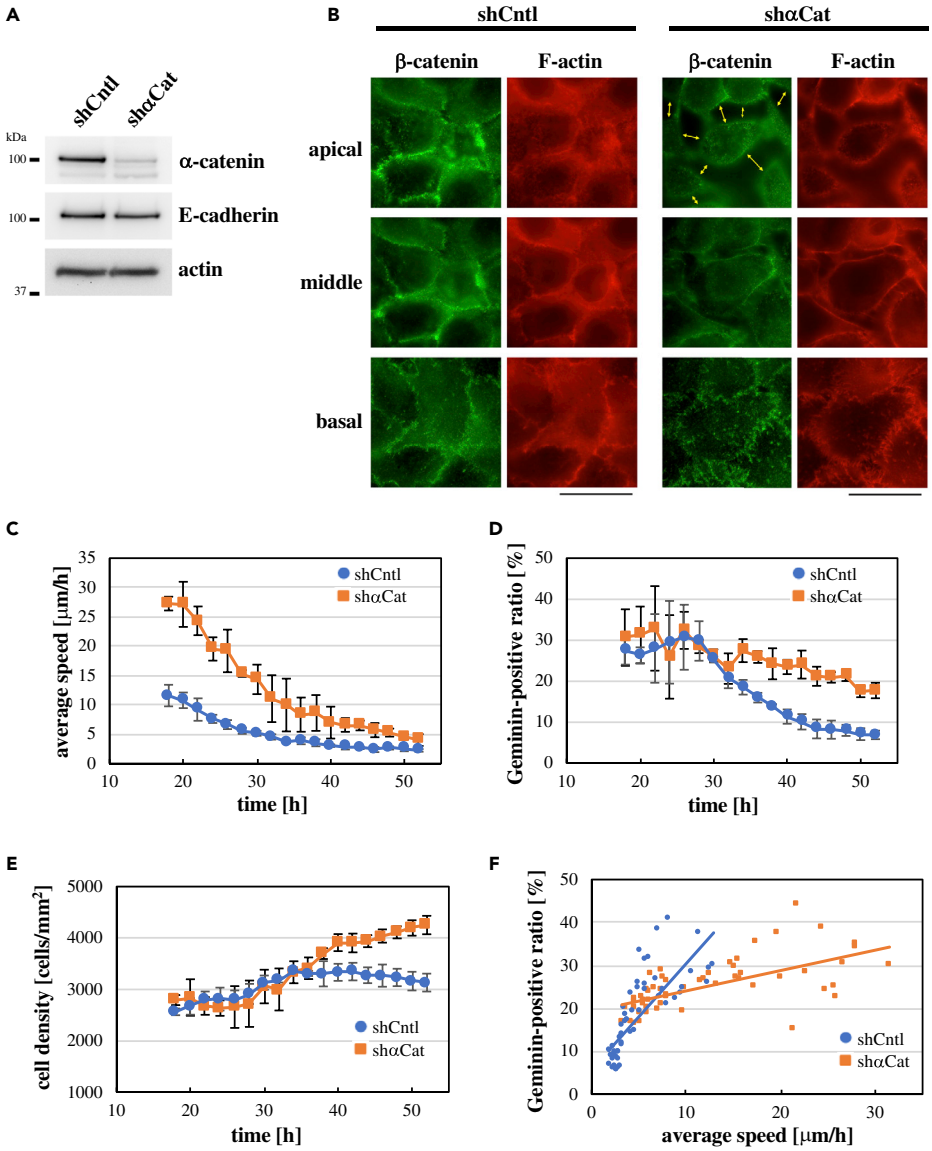

Figure 4. Effect of α-Catenin Depletion on Cell Cycle Progression and Cell Motility in Keratinocyte Sheets

(A) Validation of α-catenin depletion by immunoblotting. Short hairpin RNA (shRNA) against α-catenin (shαCat) or non-targeting shRNA (shCntl) was stably expressed in HaCaT keratinocytes.

(B) Confluent HaCaT keratinocytes expressing shRNA against α-catenin (shαCat) or non-targeting shRNA (shCntl), which were grown for 40 h after seeding cells, were stained for β-catenin and F-actin. Apical, middle, and basal focal planes of the same cells are shown for each cell type. Double-headed, yellow arrows indicate intercellular gaps observed in apical regions of α-catenin-depleted cells. Scale bars, 30 μm.

(C–E) Time-dependent changes in the average speed (C), the ratio of Geminin-positive cells against total cells (D), and the cell density (E) in keratinocyte sheets expressing either shRNA against α-catenin (shαCat) or non-targeting shRNA (shCntl) after seeding cells. Each data point represents mean ± SD. n = 3 (>100 cells at each time point in each experiment in (D)).

(F) The ratio of Geminin-positive cells was plotted against the average speed in α-catenin shRNA- or non-targeting shRNA-expressing keratinocyte sheets at each time point throughout observation. Data from three independent experiments were combined for each cell type. Regression lines of linear fitting are shown for both cell types.

See also Figures S12–S17, and Videos S9, S10, S13, and S14.

We next examined the role of Rac1 in cell cycle progression and cell motility in α-catenin-depleted keratinocytes. Rac1 inhibition decreased both the ratio of Geminin-positive cells and the cell movement speed in the early phase in α-catenin-depleted keratinocyte sheets (Figures 5A and 5B; Videos S11 and S12), being consistent with the result for normal keratinocyte sheets (Figures 3C and 3D). These results suggest that

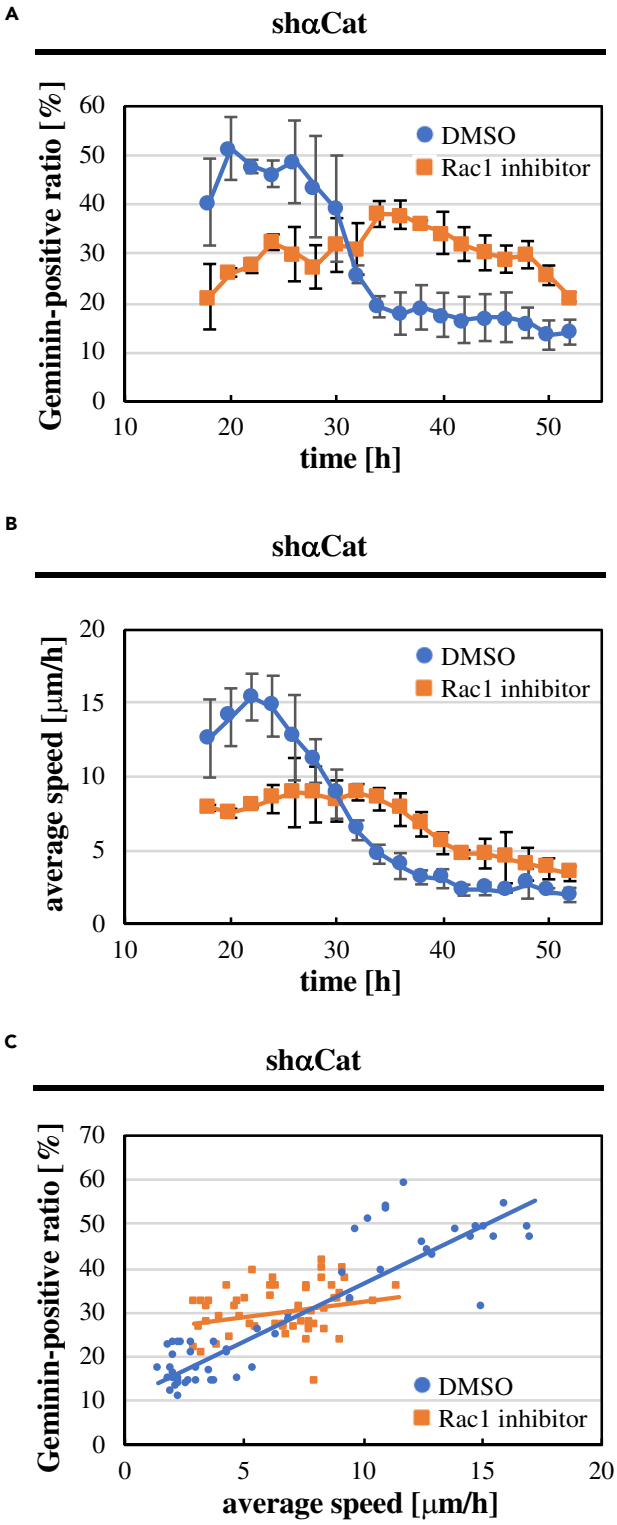

Figure 5. Role of Rac1 in Cell Cycle Progression and Cell Motility in α-Catenin-Depleted Keratinocyte Sheets

(A and B) Time-dependent changes in the ratio of Geminin-positive cells against total cells (A) and the average speed (B) in keratinocyte sheets expressing shRNA against α-catenin (shαCat) after seeding cells in the presence of DMSO (control)

Figure 5. *Continued*
or the Rac1 inhibitor (20 μM NSC23766). Each data point represents mean ± SD. n = 3 (>100 cells at each time point in each experiment in (A)).
(C) In α-catenin shRNA-expressing keratinocyte sheets under control (DMSO) and Rac1-inhibited (20 μM NSC23766) conditions, the ratio of Geminin-positive cells was plotted against the average speed at each time point throughout observation. Data from three independent experiments were combined for each condition. Regression lines of linear fitting are shown for both conditions.
See also Figures S14 and S17, and Videos S11 and S12.

Rac1 upregulates cell cycle progression and cell motility in the early phase without the aid of α-catenin-mediated intact adherens junction. Surprisingly, cell cycle progression and cell motility in α-catenin-depleted keratinocyte sheets were elevated upon Rac1 inhibition in the late phase (Figures 5A and 5B; Videos S11 and S12), even though Rac1 inhibition in normal keratinocyte sheets did not apparently affect cell cycle progression and cell motility in the late phase (Figures 3C and 3D). Consequently, Rac1 inhibition abrogated apparent correlation between cell cycle progression and cell motility in α-catenin-depleted keratinocytes (Figure 5C), which is in marked contrast to the result of Rac1 inhibition in normal keratinocyte sheets, in which Rac1 inhibition has attenuated cell cycle progression and cell motility in a coordinated manner (Figure 3E). Taken together, our results reveal that α-catenin-dependent intact cell-cell adhesion is required for Rac1-mediated coordination between cell cycle progression and cell motility in keratinocyte sheets.

The role of adherens junction was further examined by depleting extracellular Ca^{2+}, as Ca^{2+} depletion abrogates Ca^{2+}-dependent cadherin binding and concomitant formation of adherens junctions in keratinocytes (Vaezi et al., 2002). As expected, keratinocytes densely seeded in the low-Ca^{2+} medium had intercellular gaps at their apical portions (Figure S17A), which was consistent with the result of α-catenin depletion (Figure 4B). Interestingly, cell motility was highly promoted in the late time phase (later than ~30-h time point after seeding cells) under the low Ca^{2+} condition (Figure S17B; Videos S13 and S14), whereas α-catenin depletion enhanced cell motility only in the early phase (Figure 4C). Associated with this, Ca^{2+} depletion increased the ratio of Geminin-positive cells in the late phase (Figure S17C). The Rac1 activity in the late phase (50 h after seeding cells) was slightly elevated upon Ca^{2+} depletion (Figure S17D), and cell motility enhanced by Ca^{2+} depletion in this time stage was reduced by inhibition of Rac1 (Figure S17E). By contrast, Rac1 inhibition did not affect cell cycle progression in the low-Ca^{2+} medium (Figure S17F). These results show that cell motility and cell cycle progression are differentially regulated by Rac1 under the Ca^{2+}-depleted condition, which further supports the notion that intact adherens junctions are required for Rac1-mediated coordination of cell cycle progression and cell motility. It is of note that Ca^{2+} regulates not only adherens junctions but also a wide variety of molecular interactions and intracellular signaling (Yáñez et al., 2012), which may underlie the difference in actual effects of Ca^{2+} depletion and α-catenin knockdown on motile and proliferative behaviors of keratinocytes.

Cell Confluency Is Crucial for Rac1-Mediated Regulation of Cell Cycle Progression and Cell Motility

To further investigate the role of intercellular interaction in Rac1-mediated regulation of cell cycle progression and cell motility, we utilized keratinocytes seeded sparsely. In sparse cells, there was no apparent change in Rac1 activity between 30- and 50-h time points after seeding cells (Figure 6A). Associated with this, the ratio of Geminin-positive cells and the speed of cell migration were not declined into basal levels even in the late phase (i.e., later than ~30 h after seeding cells) (Figures 6B–6D; Video S15; see also Figure S4 and Video S2). When Rac1 was inhibited (Figure 6A), migration of sparse keratinocytes was largely suppressed throughout the observation period (Figures 6B and 6D; Video S16), indicating that migration of sparse keratinocytes is Rac1 dependent. By contrast, Rac1 inhibition in sparse cells gradually increased the ratio of Geminin-positive cells; almost all cells became Geminin-positive by 50 h after seeding cells (Figures 6B and 6C; Video S16). However, we noted that sparse cells under Rac1 inhibition did not show cell division (Video S16). To ascertain this, we traced cell division events for each cell from 20- to 52-h time points after seeding cells and counted the number of offspring cells that originated from a single founder cell appointed at 20-h time point (Figure 6E). As expected, in the absence of Rac1 inhibition, the number of offspring cells at 52-h time point was significantly larger under the sparse condition compared with that under the confluent condition (Figure 6F). However, Rac1 inhibition completely abrogated cell division in sparse cells, where the number of offspring cells at 52-h time point was one under this condition (Figure 6F).

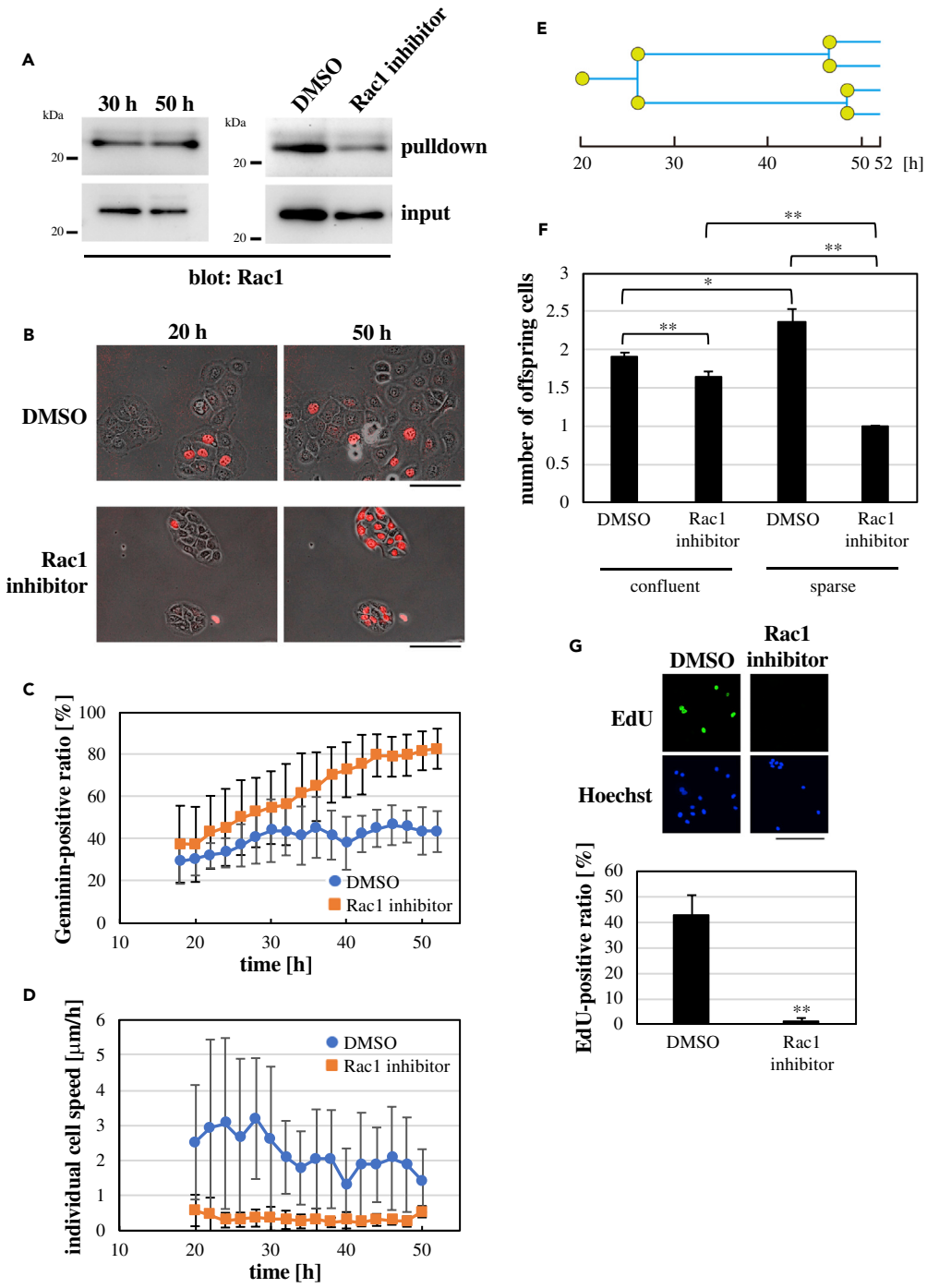

Figure 6. Role of Rac1 in Cell Cycle Progression and Cell Motility in Sparse Keratinocytes

(A) Lysates of sparse keratinocytes grown for either 30 or 50 h after seeding cells (left panel) and those grown for 30 h in the presence of DMSO (control) or the Rac1 inhibitor (20 μM NSC23766) (right panel) were subjected to the PAK1-PBD-based pull-down assay for active Rac1.

(B) Geminin-based Fucci fluorescence images (red) overlaid to phase contrast images of sparse keratinocytes at the indicated time points after seeding cells in the presence of DMSO (control) or the Rac1 inhibitor (20 μM NSC23766). Scale bars, 100 μm.

(C and D) Time-dependent changes in the ratio of Geminin-positive cells against total cells (C) and the individual cell speed (D) in sparse keratinocytes after seeding cells in the presence of DMSO (control) or the Rac1 inhibitor (20 μM

Figure 6. *Continued*
NSC23766). Each data point represents mean ± SD. n = 8 (≥ 9 cells at each time point in each experiment) in (C) and 33 in (D).
(E) A representative cell division tree of sparse keratinocytes. Originating from a single founder cell appointed at 20 h after seeding cells, 4 offspring cells were generated by 52-h time point, in this case.
(F) The number of offspring cells at 52-h time point derived from a single founder cell appointed at 20-h time point. Results of sparse and confluent cells under the control (DMSO) or Rac1-inhibited (20 μM NSC23766) condition are shown. Each bar represents mean ± SEM. n = 45 (for confluent cells) and 33 (for sparse cells). *p < 0.05, **p < 0.01 (Student's two-tailed, unpaired t test).
(G) Upper images: EdU incorporation into nuclei of sparse keratinocytes that were grown for 50 h after seeding cells in the presence of DMSO (control) or the Rac1 inhibitor (20 μM NSC23766). Total nuclei were labeled with Hoechst. Scale bar, 200 μm. Lower graph: the ratio of EdU-positive cells under the sparse condition with or without Rac1 inhibition. Each bar represents mean ± SD. n = 8 (>30 cells in each experiment). **p < 0.01 (Student's two-tailed, unpaired t test).
See also Figures S4, and Videos S2, S15, and S16.

On one hand, Rac1 inhibition under the sparse condition increased the population of cells that were in S-G_2-M phases (i.e., Geminin-positive) (Figure 6C). On the other hand, sparse cells with Rac1 inhibition did not undergo cell division (Figure 6F). These results suggest that Rac1 inhibition stops cell cycle at some stage during S-G_2-M phases in sparse keratinocytes. To address this, we examined incorporation of EdU in sparse cells and found that EdU incorporation was almost totally eliminated by inhibition of Rac1 (Figure 6G), which suggested that Rac1 inhibition arrested S phase progression in sparse cells. As mentioned earlier, Rac1 activity is likely to increase the probability of S phase entry in keratinocyte sheets. By contrast, the results for sparse cells suggest that Rac1 activity promotes S phase progression in sparse keratinocytes. Thus, cell confluency largely influences Rac1-mediated regulation of cell cycle progression in keratinocytes.

DISCUSSION

In this study, we showed that keratinocyte sheets exhibited time-dependent coordination between collective cell movement and cell cycle progression after seeding cells. Using this system, we found that Rac1 activity coordinately promoted cell motility and cell cycle progression in keratinocyte sheets. Previous studies have revealed that Rac1-dependent lamellipodia protrusion drives collective migration of keratinocytes and other types of epithelial cells both *in vitro* and *in vivo* (Fenteany et al., 2000; Tscharntke et al., 2007; Anon et al., 2012; Das et al., 2015; Park et al., 2017). Our present study shows that cell cycle progression and cell proliferation are also driven by Rac1 in keratinocyte collectives. Given that inhibition or depletion of Rac1 impairs epidermal wound repair (Tscharntke et al., 2007), coordinated promotion of cell cycle progression and cell motility by Rac1 in keratinocyte sheets may be involved in the repair, in which coordination of migration, proliferation, and differentiation of keratinocytes is crucial (Park et al., 2017).

Coupling between cell movement and cell proliferation in epithelial sheets has been typically observed in the *in vitro* wound healing assay (Streichan et al., 2014; Uroz et al., 2018). In this case, migration of leader cells into a cell-devoid region expands the epithelial sheet, causing an increase in the area of individual follower cells. The increase in the follower cell area has been suggested to induce proliferation of follower cells (Streichan et al., 2014; Uroz et al., 2018). This mechanism for coordination of cell motility and proliferation depends on the extrinsic environment of the epithelial sheet (i.e., existence of a cell-devoid region). By contrast, we show in this study that keratinocyte sheets themselves have a mechanism to coordinately promote motile and proliferative abilities of cells through Rac1 signaling. Coordinated promotion of cell cycle progression and cell motility by Rac1 did not depend on the existence of a cell-devoid region and could be observed even at a saturated cell density (Figure 1). Therefore, the increase in the individual cell area is not required for promoting cell cycle progression and cell motility by Rac1 in keratinocyte sheets. Instead, Rac1-mediated coordination of cell cycle progression and cell motility depends on adherens junction-mediated connectivity between cells.

The mechanism of how Rac1 activity promotes cell cycle progression in keratinocyte sheets is not clear yet. In skin tumors, Rac1 activates ERK through PAK1 and thereby promotes cancer cell proliferation and tumorigenesis (Wang et al., 2010). As ERK activation also promotes proliferation of keratinocytes (Shibata et al., 2012), activation of ERK may be involved in Rac1-mediated cell cycle progression and cell proliferation in keratinocyte sheets. It is noteworthy that Rac1-dependent lamellipodia protrusion and concomitant cell movement were observed before S phase entry and during S to M phase progression in keratinocyte sheets (Figures 1B and 1C; Video S5). While lamellipodia protrusion induces Ca^{2+} influx through mechano-sensitive ion channels (MS channels) (Wei et al., 2009), the MS channel-mediated intracellular [Ca^{2+}] increase is

known to promote cell cycle progression and proliferation in various cell types including keratinocytes (Liu et al., 1994; Yano et al., 2004; Gudipaty et al., 2017). Therefore, Rac1-dependent lamellipodia protrusion and concomitant Ca^{2+} influx may also contribute to cell cycle progression in keratinocyte sheets. This idea is consistent with the recent study showing that formation of cortical actin network mediated by the Rac1-WAVE-Arp2/3 pathway is required for cell cycle progression and cell proliferation in sparse mammary epithelial cells (Molinie et al., 2019). Furthermore, we found in this study that depletion of extracellular Ca^{2+} eliminated the transient increase in the ratio of Geminin-positive cells that was observed under the normal medium condition around 30 h after seeding cells (Figure S17C).

It is well known that normal epithelial cells including keratinocytes exhibit contact inhibition of proliferation and locomotion, wherein cell proliferation and motility are arrested under the confluent condition (Mayor and Carmona-Fontaine, 2010; McClatchey and Yap, 2012; Puliafito et al., 2012; Hirata et al., 2017; Lång et al., 2018). Recent studies have suggested that the cell-crowding-induced decrease in individual cell area is responsible for arresting cell proliferation in epithelial monolayers (Puliafito et al., 2012; Aragona et al., 2013; Streichan et al., 2014; Uroz et al., 2018). Consistent with this, we observed in keratinocyte sheets that cell cycle progression, as well as cell motility, was attenuated with an increase in the cell density (i.e., with a decrease in the individual cell area) in the time phase earlier than ~30 h after seeding cells (Figures 1F–1H, and S6). However, even at the saturated level of cell density, cell cycle and cell motility were not fully arrested in the early time phase, and approximately 50 h were required for full arrests in cell cycle and cell motility (Figures 1F–1H, and S6). These results suggest that the cell density or the individual cell area is not a sole determinant of cell cycle progression and cell motility in keratinocyte sheets, and some additional time-dependent factor is involved in the regulations of these cellular activities. In this study, we have revealed that whereas cell cycle progression and cell motility in the early phase are promoted by Rac1, their attenuation in the late phase (later than ~30 h after seeding cells) is associated with a decline in the Rac1 activity. Therefore, it is conceivable that the time course of Rac1 deactivation may dictate the time point for onset of arrests in cell cycle and cell motility. On the other hand, we have recently revealed that RhoA-dependent actomyosin tension at adherens junctions is required for arresting cell proliferation in confluent keratinocytes (Hirata et al., 2017). Considering that Rac1 and RhoA pathways antagonize each other (Rottner et al., 1999; Chauhan et al., 2011), transition from the Rac1-dominated regime to the RhoA-dominated one may occur in the late phase to achieve arrests in cell cycle and cell motility in keratinocyte sheets. Translocation of p120 catenin from a cytoplasmic pool to cadherin-mediated adhesions may be involved in the transition from Rac1 to RhoA regimes (Anastasiadis et al., 2000; Noren et al., 2000; Anastasiadis and Reynolds, 2001). However, the actual factor(s) that determines the time course of Rac1 deactivation (or RhoA activation) in keratinocyte sheets is currently unknown and needs to be revealed in future studies.

Our results suggest that Rac1 drives cell cycle progression in keratinocyte sheets by promoting S phase entry. This is consistent with previous studies showing Rac1-dependent S phase entry in a variety of cell types (Mettouchi et al., 2001; Matos and Jordan, 2005; Li et al., 2011). On the contrary, Rac1 activity is not likely to be essential for S phase entry but is required for S phase progression in sparse keratinocytes. Although the actual mechanism underlying Rac1-dependent progression of S phase under the sparse condition is unclear, topoisomerase II-mediated DNA cleavage, an essential step in DNA replication (Wang et al., 2002), may be promoted by the Rac1-PAK pathway (Huelsenbeck et al., 2012). Nonetheless, it is totally unknown at present how difference in cell confluency leads to alternation in the target point of Rac1 in the cell cycle. Future studies addressing this matter will provide mechanistic insights into how behaviors of collective and individual cells are distinctively regulated by Rac1.

Limitations of the Study

In this study, we find that keratinocyte sheets exhibit time-dependent coordination of collective cell movement and cell cycle progression after seeding cells. Rac1 promotes both cell motility and cell cycle progression in the early phase, and attenuation of these cellular activities in the late time phase is associated with a decline in the Rac1 activity. Furthermore, adherens junction-mediated cell-cell adhesion is required for the coordinated regulation of cell cycle and cell motility by Rac1. However, there remain two major questions. What determines the time-dependent change in the Rac1 activity? How do adherens junctions coordinate cell cycle progression and cell motility without affecting the Rac1 activity? Future studies addressing these points will substantially advance our mechanistic understanding of collective behaviors of cells.

Resource Availability

Lead Contact

Further information and requests for reagents should be directed to and will be fulfilled by the Lead Contact, Hiroaki Hirata (hhirata@med.nagoya-u.ac.jp).

Materials Availability

Plasmid constructs generated in this study are available from the Lead Contact on request.

Data and Code Availability

This study did not generate any unique code or software. The published article includes all datasets generated during this study.

METHODS

All methods can be found in the accompanying Transparent Methods supplemental file.

SUPPLEMENTAL INFORMATION

Supplemental Information can be found online at https://doi.org/10.1016/j.isci.2020.101729.

ACKNOWLEDGMENTS

We thank Michiyuki Matsuda (Kyoto University, Japan), Michael J. Schell (Uniformed Services University, USA), Kozo Kaibuchi (Nagoya University, Japan), Toshio Kitamura (University of Tokyo, Japan), Shigenobu Yonemura (Tokushima University, Japan), and Keiko Kawauchi (Konan University, Japan) for the kind gifts of DNA constructs. This work was supported by the grant for collaborative research between Nagoya University and R-Pharm (2614Dj-02b to M.S.) and JSPS KAKENHI (19K23748 to H.H., 20K12596 to H.H., and 15H05936 to M.S.).

AUTHOR CONTRIBUTIONS

Conceptualization, H.H. and M.S.; Methodology, H.H.; Investigation, H.H. and O.D.; Formal Analysis, H.H.; Writing – Original Draft, H.H.; Writing – Review & Editing, M.S.; Funding Acquisition, H.H. and M.S.

DECLARATION OF INTERESTS

The authors declare no competing financial interests.

Received: October 29, 2019
Revised: January 23, 2020
Accepted: October 21, 2020
Published: November 20, 2020

REFERENCES

Aman, A., and Piotrowski, T. (2010). Cell migration during morphogenesis. Dev. Biol. *341*, 20–33.

Anastasiadis, P.Z., Moon, S.Y., Thoreson, M.A., Mariner, D.J., Crawford, H.C., Zheng, Y., and Reynolds, A.B. (2000). Inhibition of RhoA by p120 catenin. Nat. Cell Biol. *2*, 637–644.

Anastasiadis, P.Z., and Reynolds, A.B. (2001). Regulation of Rho GTPases by p120-catenin. Curr. Opin. Cell Biol. *13*, 604–610.

Anon, E., Serra-Picamal, X., Hersen, P., Gauthier, N.C., Sheetz, M.P., Trepat, X., and Ladoux, B. (2012). Cell crawling mediates collective cell migration to close undamaged epithelial gaps. Proc. Natl. Acad. Sci. U S A *109*, 10891–10896.

Aragona, M., Panciera, T., Manfrin, A., Giulitti, S., Michielin, F., Elvassore, N., Dupont, S., and Piccolo, S. (2013). A mechanical checkpoint controls multicellular growth through YAP/TAZ regulation by actin-processing factors. Cell *154*, 1047–1059.

Cai, D., Chen, S.C., Prasad, M., He, L., Wang, X., Choesmel-Cadamuro, V., Sawyer, J.K., Danuser, G., and Montell, D.J. (2014). Mechanical feedback through E-cadherin promotes direction sensing during collective cell migration. Cell *157*, 1146–1159.

Chauhan, B.K., Lou, M., Zheng, Y., and Lang, R.A. (2011). Balanced Rac1 and RhoA activities regulate cell shape and drive invagination morphogenesis in epithelia. Proc. Natl. Acad. Sci. U S A *108*, 18289–18294.

Das, T., Safferling, K., Rausch, S., Grabe, N., Boehm, H., and Spatz, J.P. (2015). A molecular mechanotransduction pathway regulates collective migration of epithelial cells. Nat. Cell Biol. *17*, 276–287.

Fenteany, G., Janmey, P.A., and Stossel, T.P. (2000). Signaling pathway and cell mechanics involved in wound closure by epithelial cell sheets. Curr. Biol. *10*, 831–838.

Friedl, P., and Gilmour, D. (2009). Collective cell migration in morphogenesis, regeneration and cancer. Nat. Rev. Mol. Cell Biol. *10*, 445–457.

Gao, Y., Dickerson, B., Guo, F., Zheng, J., and Zheng, Y. (2004). Rational design and characterization of a Rac GTPase-specific small molecule inhibitor. Proc. Natl. Acad. Sci. U S A *101*, 7618–7623.

Garcia-Hughes, G., Link, N., Ghosh, A.B., and Abrams, J.M. (2015). Hid arbitrates collective cell death in the Drosophila wing. Mech. Dev. *138*, 349–355.

Gudipaty, S.A., Lindblom, J., Loftus, P.D., Redd, M.J., Edes, K., Davey, C.F., Krishnegowda, V., and Rosenblatt, J. (2017). Mechanical stretch triggers rapid epithelial cell division through Piezo1. Nature *543*, 118–121.

Hariharan, I.K. (2015). Organ size control: lessons from Drosophila. Dev. Cell *34*, 255–265.

Hirata, H., Samsonov, M., and Sokabe, M. (2017). Actomyosin contractility provokes contact inhibition in E-cadherin-ligated keratinocytes. Sci. Rep. *7*, 46326.

Huelsenbeck, S.C., Schorr, A., Roos, W.P., Huelsenbeck, J., Henninger, C., Kaina, B., and Fritz, G. (2012). Rac1 protein signaling is required for DNA damage response stimulated by topoisomerase II poisons. J. Biol. Chem. *287*, 38590–38599.

Komatsu, N., Aoki, K., Yamada, M., Yukinaga, H., Fujita, Y., Kamioka, Y., and Matsuda, M. (2011). Development of an optimized backbone of FRET biosensors for kinases and GTPases. Mol. Biol. Cell *22*, 4647–4656.

Kurokawa, K., Itoh, R.E., Yoshizaki, H., Ohba, Y., Nakamura, T., and Matsuda, M. (2004). Coactivation of Rac1 and Cdc42 at lamellipodia and membrane ruffles induced by epidermal growth factor. Mol. Biol. Cell *15*, 1003–1010.

Lång, E., Połec, A., Lång, A., Valk, M., Blicher, P., Rowe, A.D., Tønseth, K.A., Jackson, C.J., Utheim, T.P., Janssen, L.M.C., et al. (2018). Coordinated collective migration and asymmetric cell division in confluent human keratinocytes without wounding. Nat. Commun. *9*, 3665.

Lecuit, T., and Le Goff, L. (2007). Orchestrating size and shape during morphogenesis. Nature *450*, 189–192.

Leevers, S.J., and McNeill, H. (2005). Controlling the size of organs and organisms. Curr. Opin. Cell Biol. *17*, 604–609.

Li, A., Ma, Y., Yu, X., Mort, R.L., Lindsay, C.R., Stevenson, D., Strathdee, D., Insall, R.H., Chernoff, J., Snapper, S.B., et al. (2011). Rac1 drives melanoblast organization during mouse development by orchestrating pseudopod-driven motility and cell-cycle progression. Dev. Cell *21*, 722–734.

Liu, W.F., Nelson, C.M., Pirone, D.M., and Chen, C.S. (2006). E-cadherin engagement stimulates proliferation via Rac1. J. Cell Biol. *173*, 431–441.

Liu, M., Xu, J., Tanswell, A.K., and Post, M. (1994). Inhibition of mechanical strain-induced fetal rat lung cell proliferation by gadolinium, a stretch-activated channel blocker. J. Cell. Physiol. *161*, 501–507.

Matos, P., and Jordan, P. (2005). Expression of Rac1b stimulates NF-κB-mediated cell survival and G1/S progression. Exp. Cell Res. *305*, 292–299.

Mayor, R., and Carmona-Fontaine, C. (2010). Keeping in touch with contact inhibition of locomotion. Trends Cell Biol. *20*, 319–328.

McClatchey, A.I., and Yap, A.S. (2012). Contact inhibition (of proliferation) redux. Curr. Opin. Cell Biol. *24*, 685–694.

Mettouchi, A., Klein, S., Guo, W., Lopez-Lago, M., Lemichez, E., Westwick, J.K., and Giancotti, F.G. (2001). Integrin-specific activation of Rac controls progression through the G_1 phase of the cell cycle. Mol. Cell *8*, 115–127.

Molinie, N., Rubtsova, S.N., Fokin, A., Visweshwaran, S.P., Rocques, N., Polesskaya, A., Schnitzler, A., Vacher, S., Denisov, E.V., Tashireva, L.A., et al. (2019). Cortical branched actin determines cell cycle progression. Cell Res. *29*, 432–445.

Moore, K.A., Sethi, R., Doanes, A.M., Johnson, T.M., Pracyk, J.B., Kirby, M., Irani, K., Goldschmidt-Clermont, P.J., and Finkel, T. (1997). Rac1 is required for cell proliferation and G2/M progression. Biochem. J. *326*, 17–20.

Ng, M.R., Besser, A., Danuser, G., and Brugge, J.S. (2012). Substrate stiffness regulates cadherin-dependent collective migration through myosin-II contractility. J. Cell Biol. *199*, 545–563.

Noren, N.K., Liu, B.P., Burridge, K., and Kreft, B. (2000). p120 catenin regulates the actin cytoskeleton via Rho family GTPases. J. Cell Biol. *150*, 567–579.

Olson, M.F., Ashworth, A., and Hall, A. (1995). An essential role for Rho, Rac, and Cdc42 GTPases in cell cycle progression through G_1. Science *269*, 1270–1272.

Pan, D. (2007). Hippo signaling in organ size control. Genes Dev. *21*, 886–897.

Park, S., Gonzalez, D.G., Guirao, B., Boucher, J.D., Cockburn, K., Marsh, E.D., Mesa, K.R., Brown, S., Rompolas, P., Haberman, A.M., et al. (2017). Tissue-scale coordination of cellular behaviour promotes epidermal wound repair in live mice. Nat. Cell Biol. *19*, 155–163.

Puliafito, A., Hufnagel, L., Neveu, P., Streichan, S., Sigal, A., Fygenson, D.K., and Shraiman, B.I. (2012). Collective and single cell behavior in epithelial contact inhibition. Proc. Natl. Acad. Sci. U S A *109*, 739–744.

Ridley, A.J., Paterson, H.F., Johnston, C.L., Diekmann, D., and Hall, A. (1992). The small GTP-binding protein rac regulates growth factor-induced membrane ruffling. Cell *70*, 401–410.

Rottner, K., Hall, A., and Small, J.V. (1999). Interplay between Rac and Rho in the control of substrate contact dynamics. Curr. Biol. *9*, 640–648.

Sakaue-Sawano, A., Kurokawa, H., Morimura, T., Hanyu, A., Hama, H., Osawa, H., Kashiwagi, S., Fukami, K., Miyata, T., Miyoshi, H., et al. (2008). Visualizing spatiotemporal dynamics of multicellular cell-cycle progression. Cell *132*, 487–498.

Shaw, T.J., and Martin, P. (2009). Wound repair at a glance. J. Cell Sci. *122*, 3209–3213.

Shibata, S., Tada, Y., Asano, Y., Hau, C.S., Kato, T., Saeki, H., Yamauchi, T., Kubota, N., Kadowaki, T., and Sato, S. (2012). Adiponectin regulates cutaneous wound healing by promoting keratinocyte proliferation and migration via the ERK signaling pathway. J. Immunol. *189*, 3231–3241.

Streichan, S.J., Hoerner, C.R., Schneidt, T., Holzer, D., and Hufnagel, L. (2014). Spatial constraints control cell proliferation in tissues. Proc. Natl. Acad. Sci. U S A *111*, 5586–5591.

Tscharntke, M., Pofahl, R., Chrostek-Grashoff, A., Smyth, N., Niessen, C., Niemann, C., Hartwig, B., Herzog, V., Klein, H.W., Krieg, T., et al. (2007). Impaired epidermal wound healing in vivo upon inhibition or deletion of Rac1. J. Cell Sci. *120*, 1480–1490.

Uroz, M., Wistorf, S., Serra-Picamal, X., Conte, V., Sales-Pardo, M., Roca-Cusachs, P., Guimerà, R., and Trepat, X. (2018). Regulation of cell cycle progression by cell-cell and cell-matrix forces. Nat. Cell Biol. *20*, 646–654.

Vaezi, A., Bauer, C., Vasioukhin, V., and Fuchs, E. (2002). Actin cable dynamics and Rho/Rock orchestrate a polarized cytoskeletal architecture in the early steps of assembling a stratified epithelium. Dev. Cell *3*, 367–381.

Vedula, S.R.K., Hirata, H., Nai, M.H., Brugués, A., Toyama, Y., Trepat, X., Lim, C.T., and Ladoux, B. (2014). Epithelial bridges maintain tissue integrity during collective cell migration. Nat. Mater. *13*, 87–96.

Wang, J.C. (2002). Cellular roles of DNA topoisomerases: a molecular perspective. Nat. Rev. Mol. Cell Biol. *3*, 430–440.

Wang, Z., Pedersen, E., Basse, A., Lefever, T., Peyrollier, K., Kapoor, S., Mei, Q., Karlsson, R., Chrostek-Grashoff, A., and Brakebusch, C. (2010). Rac1 is crucial for Ras-dependent skin tumor formation by controlling Pak1-Mek-Erk hyperactivation and hyperproliferation in vivo. Oncogene *29*, 3362–3373.

Wei, C., Wang, X., Chen, M., Ouyang, K., Song, L.S., and Cheng, H. (2009). Calcium flickers steer cell migration. Nature *457*, 901–905.

Yáñez, M., Gil-Longo, J., and Campos-Toimil, M. (2012). Calcium binding proteins. Adv. Exp. Med. Biol. *740*, 461–482.

Yano, S., Komine, M., Fujimoto, M., Okochi, H., and Tamaki, K. (2004). Mechanical stretching in vitro regulates signal transduction pathways and cellular proliferation in human epidermal keratinocytes. J. Invest. Dermatol. *122*, 783–790.

iScience, Volume *23*

Supplemental Information

Coordination between Cell Motility and Cell Cycle Progression in Keratinocyte Sheets via Cell-Cell Adhesion and Rac1

Hiroaki Hirata, Oleg Dobrokhotov, and Masahiro Sokabe

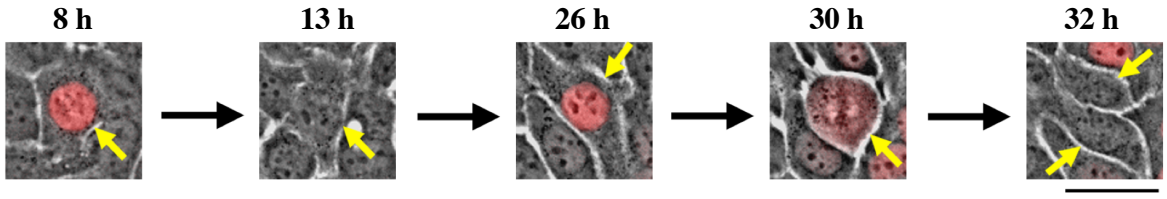

Figure S1. Time-dependent relationship between Geminin-based Fucci signal and cell division (Related to Figure 1). Geminin-based Fucci fluorescence images (red) overlaid to phase contrast images of a single cell and its daughter cells (yellow arrows) in a keratinocyte sheet at indicated time after seeding cells. Note that the Geminin signal at 8 h disappeared by 13-h time point without cell division. Scale bar: 30 μm.

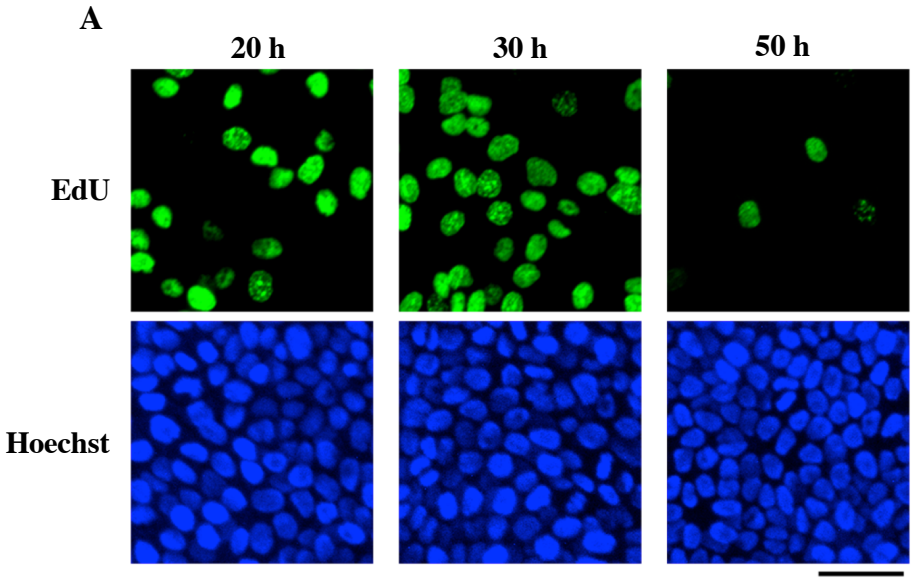

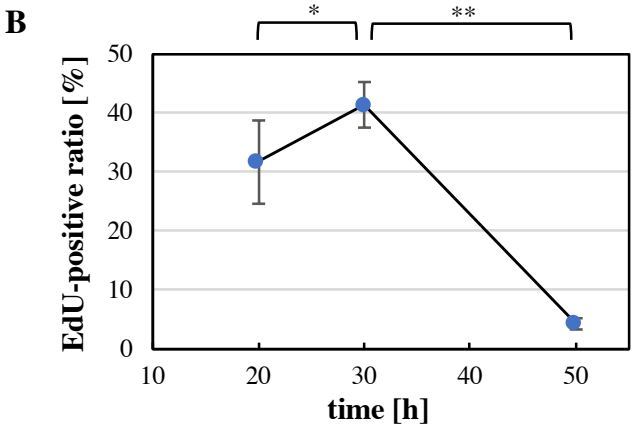

Figure S2. Time-dependent change in EdU incorporation into nuclei in keratinocyte sheets (Related to Figure 1). (A) EdU incorporation into nuclei in keratinocyte sheets that were grown for indicated time after seeding cells. Total nuclei were labeled with Hoechst. Scale bar: 50 μm. (B) Time-dependent change in the ratio of EdU-positive cells in keratinocyte sheets after seeding cells. Each data point represents mean ± SD. n = 7 (> 100 cells in each experiment). *$P < 0.05$; **$P < 0.01$ (Student's two-tailed, unpaired *t*-test).

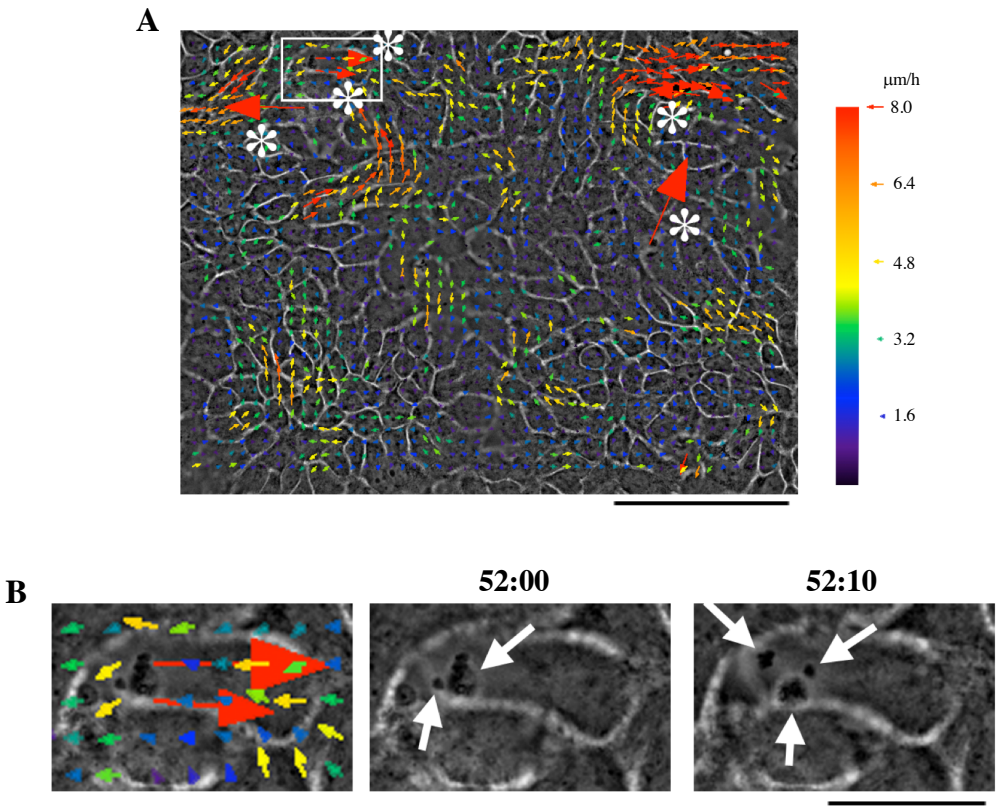

Figure S3. Floating extracellular particles cause appearance of aberrant vectors in PIV (Related to Figure 1). (A) A velocity vector map for a keratinocyte sheet at 52 h after seeding cells was overlaid to its phase contrast image. Aberrantly large vectors are indicated by asterisks. Scale bar: 100 μm. (B) Left panel: an enlarged image of the boxed region in (A). Middle and right panels: two consecutive phase contrast images (at time points of 52 h and 52 h 10 min after seeding cells) that were used for PIV calculation shown in (A). Only the region same as that in the left panel is shown. Floating extracellular particles are indicated by white arrows. See **Transparent Methods** for details. Scale bar: 30 μm.

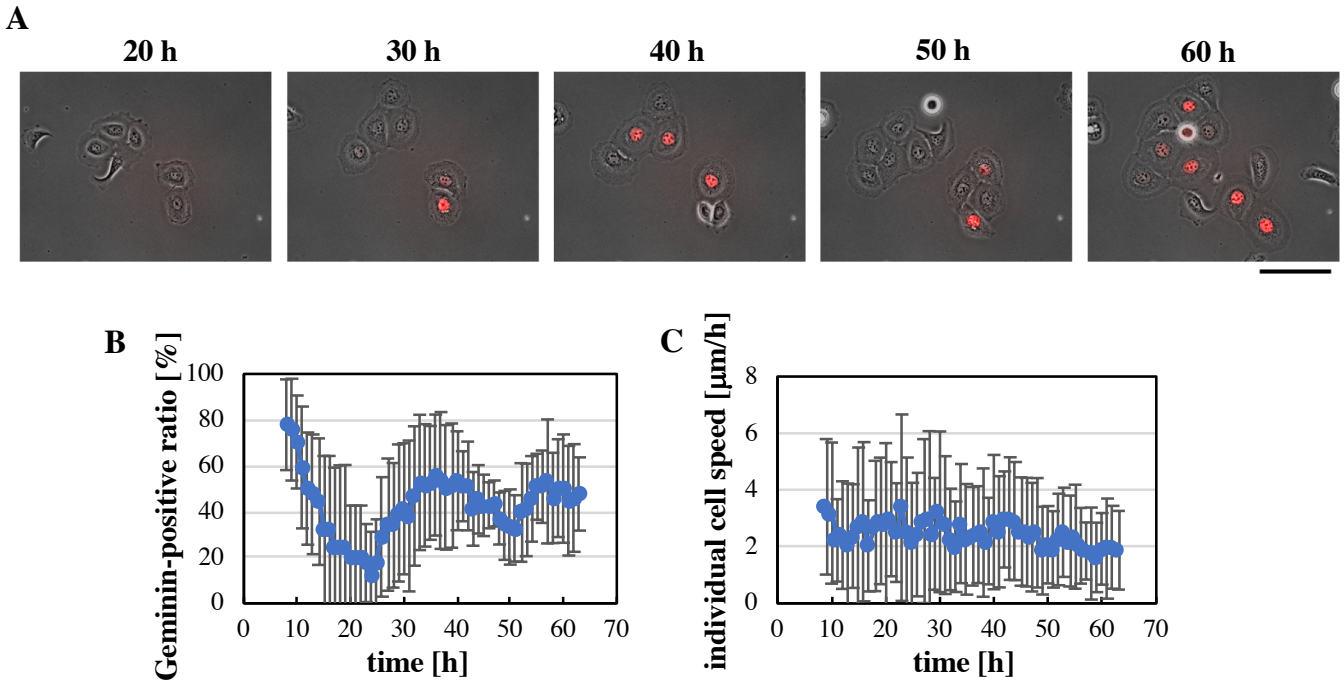

Figure S4. Time-dependent changes in cell cycle progression and cell motility in sparse keratinocytes (Related to Figures 1 and 6). (A) Geminin-based Fucci fluorescence images (red) at indicated time after seeding cells were overlaid to phase contrast images of sparse keratinocytes. Scale bar: 100 μm. (B and C) Time-dependent changes in the ratio of Geminin-positive cells against total cells (B) and the individual cell speed (C) in sparse keratinocytes after seeding cells. Each data point represents mean ± SD. n = 8 (≥ 5 cells at each time point in each experiment) in (B) and 33 in (C).

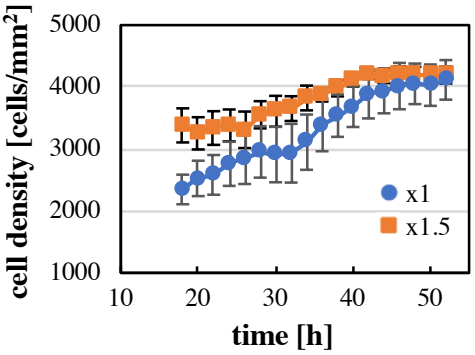

Figure S5. Time-dependent change of the cell density in H2B-GFP-expressing keratinocyte sheets after seeding different numbers of cells (Related to Figure 1). The numbers of seeded cells were 20 x 10^5 cells for 'x1' and 30 x 10^5 cells for 'x1.5'. Cell densities were quantified by counting H2B-GFP-labeled nuclei. Each data point represents mean ± SD. n = 3.

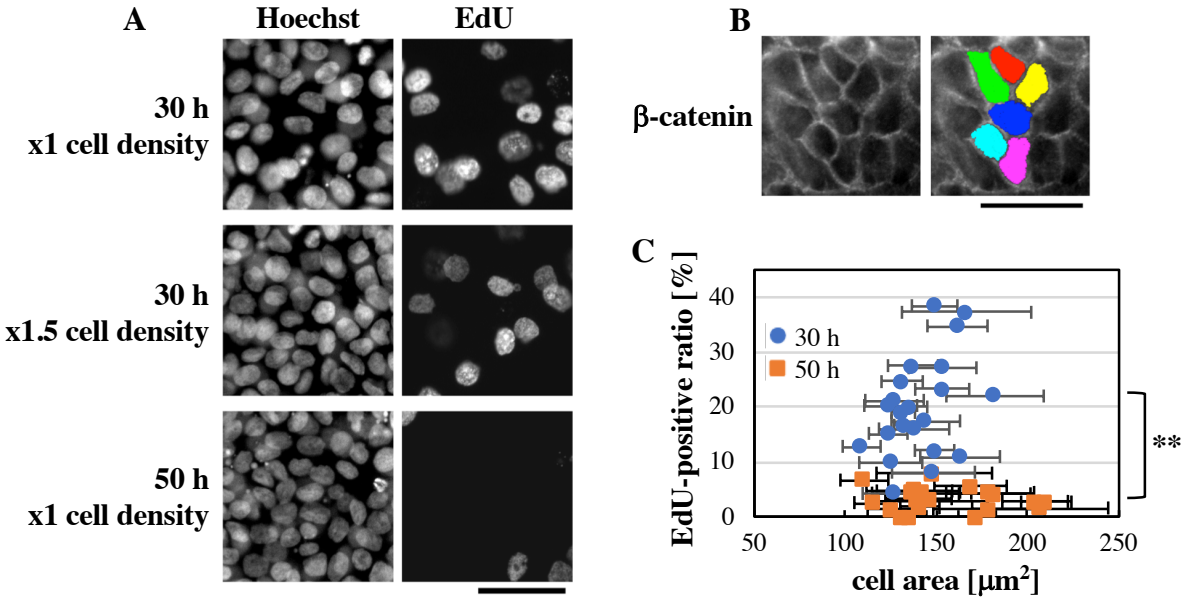

Figure S6. Effects of culture duration and cell density on nuclear incorporation of EdU in keratinocyte sheets (Related to Figure 1). (A) Keratinocyte sheets applied with EdU at the indicated time after seeding cells were fixed and stained for nuclei with Hoechst. The numbers of seeded cells were 20 x 10^5 cells for "x1" and 30 x 10^5 cells for "x1.5". Scale bar: 50 μm. (B) Measurement of individual cell areas in β-catenin-stained keratinocyte sheets. Scale bar: 50 μm. (C) Relationship between nuclear incorporation of EdU and the individual cell area in keratinocyte sheets at 30-h and 50-h time points after seeding cells. Individual cell areas and the ratio of EdU-positive cells were quantified in 22 regions (for "30 h") or 20 regions (for "50 h") of 3 keratinocyte sheets with different cell seeding densities, where each region contained > 50 cells. The individual cell area in each region is represented by mean ± SD. The ratio of EdU-positive cells at 30-h time point was significantly lower than that at 50-h time point (**P < 0.01; Student's two-tailed, unpaired t-test).

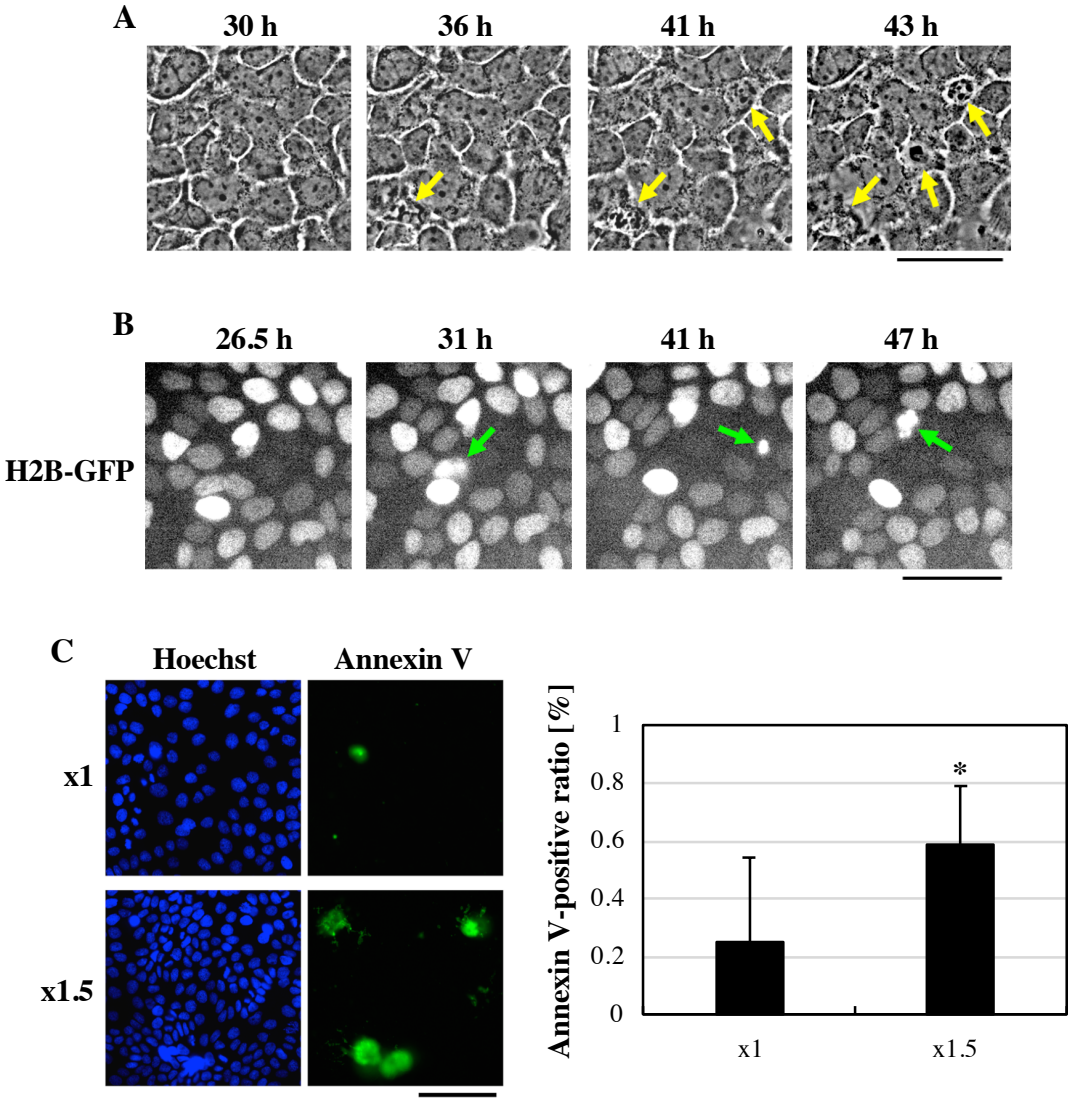

Figure S7. Cell death observed in the late time phase in keratinocyte sheets with a high cell seeding density (Related to Figure 1). (A) Phase contrast images of a keratinocyte sheet at indicated time points after seeding cells (30 x 10^5 cells seeded). Yellow arrows indicate dead cells. Scale bar: 50 μm. (B) Fluorescence images of an H2B-GFP-expressing keratinocyte sheet at indicated time points after seeding cells (30 x 10^5 cells seeded). Green arrows indicate dead cells with condensed nuclei. Scale bar: 50 μm. (C) Keratinocyte sheets with different cell seeding densities were grown for 40 h and treated with FITC-labelled Annexin V and Hoechst 33342. The numbers of seeded cells were 20 x 10^5 cells for "x1" and 30 x 10^5 cells for "x1.5". Left panels: fluorescence images of Hoechst-stained nuclei and cell-surface-bound Annexin V in the keratinocyte sheets. Scale bar: 100 μm. Right graph: the ratio of Annexin V-positive cells in the keratinocyte sheets. Each bar represents mean ± SD. n = 8 (> 300 cells each). *$P < 0.05$ (Student's two-tailed, unpaired *t*-test).

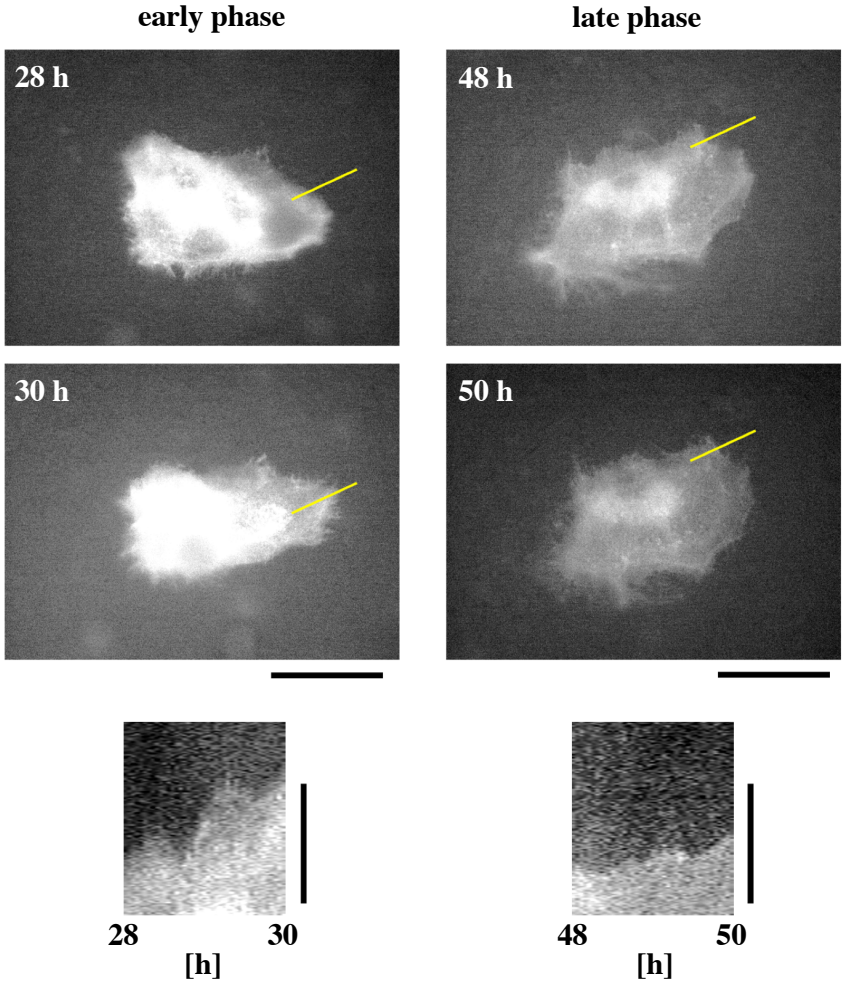

Figure S8. Kymograph analysis of the protrusive activity of keratinocytes in keratinocyte sheets (Related to Figure 2). HaCaT cells expressing F-tractin-GFP were sparsely mixed with naïve HaCaT cells and seeded to form a keratinocyte sheet. A single F-tractin-GFP-expressing cell in a sheet was tracked. Upper four panels show snapshots of an F-tractin-GFP-expressing cell at indicated time points after seeding cells. Lower two panels represent kymographs created along yellow lines in the upper snapshots. Protruding regions of the cell in early (from 28- to 30-h time points) and late (from 48- to 50-h time points) time phases were analyzed. Scale bars: 50 μm for snapshots and 20 μm for kymographs.

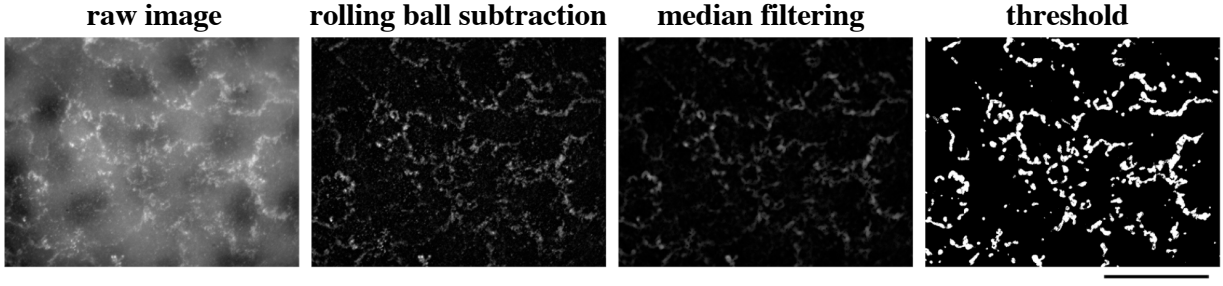

Figure S9. Image processing to extract cortactin-positive lamellipodia regions (Related to Figure 2). A immunofluorescence image of cortactin (raw image) was subjected to rolling ball subtraction of the background staining. Tiny dots outside wavy lamellipodia were then removed by median filtering. In the resultant image, lamellipodia regions were extracted by setting a threshold level. Scale bar: 30 μm.

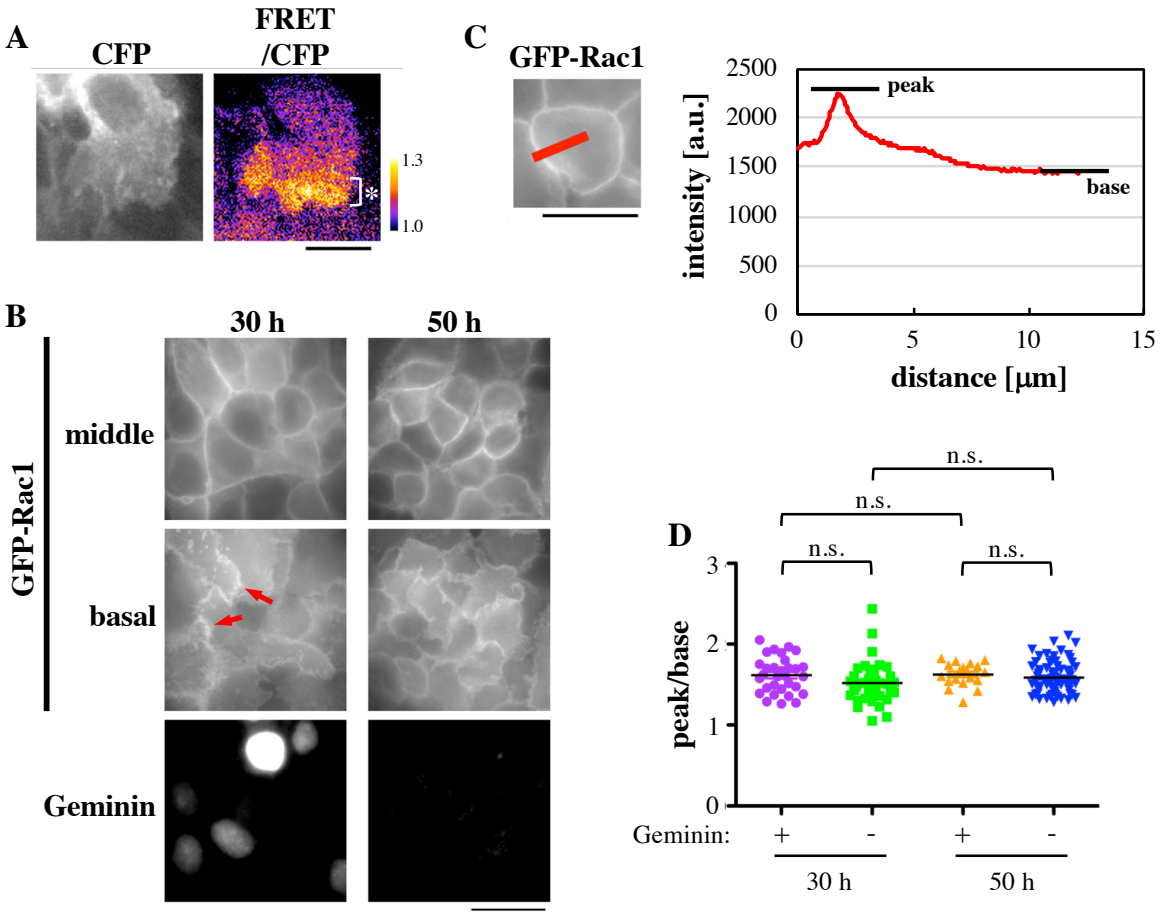

Figure S10. Localization of Rac1 in keratinocyte sheets (Related to Figure 2). (A) CFP and FRET/CFP ratio images of a RaichuEV-Rac-expressing keratinocyte in a keratinocyte sheet. An asterisk indicates the lamellipodia region with high Rac1 activity. Scale bar: 20 μm. (B) Keratinocyte sheets introduced with the Geminin-based Fucci probe and GFP-Rac1 were fixed and observed at 30-h and 50-h time points after seeding cells. For GFP-Rac1, middle and basal focal planes are shown. Red arrows indicate accumulation of GFP-Rac1 at lamellipodia tips. Scale bar: 30 μm. (C) The method for analyzing Rac1 localization at the cell-cell boundary. Fluorescence intensities of GFP-Rac1 along a line crossing the cell-cell boundary (red line in the left panel) were measured. Then, the peak intensity at the cell-cell boundary and the base intensity in the internal region of the cell were obtained (right graph). The ratio of the peak intensity against the base intensity was used as a index for relative localization of Rac1 at the cell-cell boundary. (D) The peak/base intensity ratio of GFP-Rac1 was calculated for cells grown for 30 h or 50 h after seeding cells. Geminin-positive cells and Geminin-negative ones were analyzed separately. n = 31 (30 h, Geminin-positive), 39 (30 h, Geminin-negative), 19 (50 h, Geminin-positive) and 69 (50 h, Geminin-negative). n.s., no significant difference (Student's two-tailed, unpaired *t*-test).

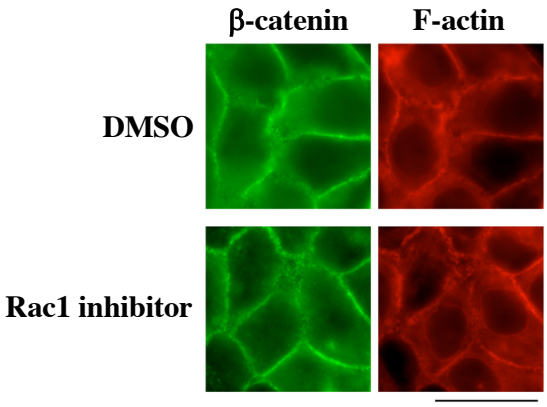

Figure S11. Effect of Rac1 inhibition on formation of adherens junctions (Related to Figure 3). Keratinocyte sheets formed in the presence of DMSO (control) or the Rac1 inhibitor (20 μM NSC23766) were fixed at 30 h after seeding cells and stained for β-catenin and F-actin. Scale bar: 30 μm.

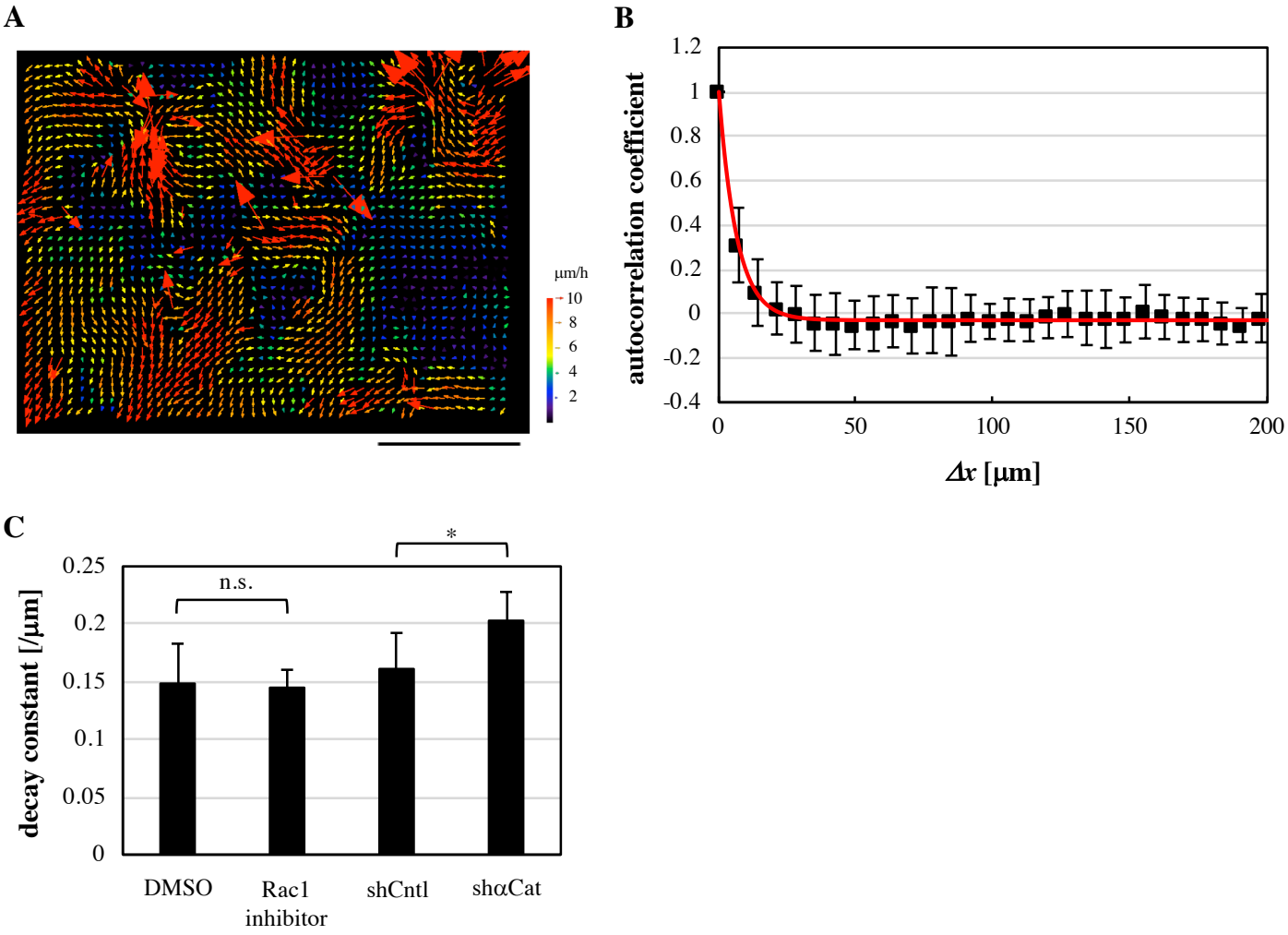

Figure S12. Spatial autocorrelation analysis of cell movement direction in keratinocyte sheets (Related to Figures 3 and 4). (A) A typical velocity vector map for keratinocyte sheets at 20 h after seeding cells. Scale bar: 100 μm. (B) Spatial autocorrelation for distribution of vector angles in the velocity vector map shown in (A) was analyzed. Correlogram of the spatial autocorrelation against Δx is shown. Each plot represents the averaged autocorrelation coefficient ± SD (n = 35). The plots were fitted with the equation [1] (red line). See **Transparent Methods** for details. (C) Decay constants in regression curves of correlograms with the equation [1] were calculated for keratinocyte sheets at 20 h after seeding cells. Keratinocyte sheets treated with the Rac1 inhibitor (20 μM NSC23766) or the vehicle only (DMSO), and keratinocyte sheets expressing shRNA against α-catenin (shαCat) or non-targeting shRNA (shCntl) were analyzed. The larger the decay constant is, the shorter the correlation length of spatial distribution of velocity vector angles is, and, therefore, the less collective the cell movement in the keratinocyte sheet is. Each bar represents mean ± SD. n = 6. *$P < 0.05$; n.s., no significant difference (Student's two-tailed, unpaired *t*-test).

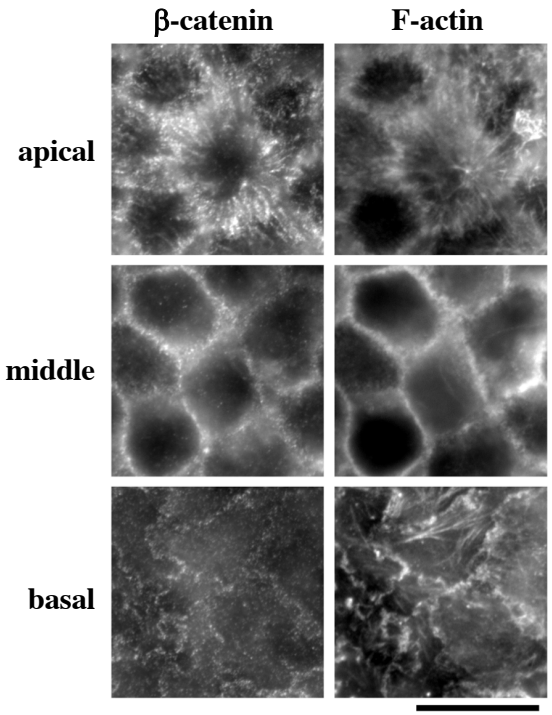

Figure S13. Assemblies of β-catenin and F-actin at different focal planes of a keratinocyte sheet (Related to Figure 4). A keratinocyte sheet at 50 h after seeding cells was stained for β-catenin and F-actin. Apical, middle and basal focal planes of the keratinocyte sheet are shown. Scale bar: 20 μm.

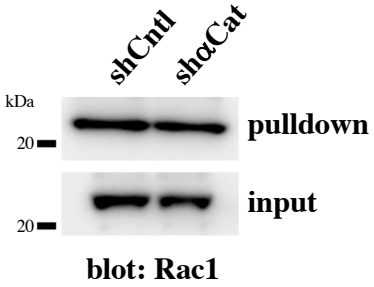

Figure S14. Depletion of α-catenin does not alter the Rac1 activity (Related to Figures 4 and 5). Keratinocyte sheets expressing shRNA against α-catenin (shαCat) or non-targeting shRNA (shCntl) were grown for 30 h after seeding cells. Their lysates were subjected to the PAK1-PBD-based pulldown assay for active Rac1.

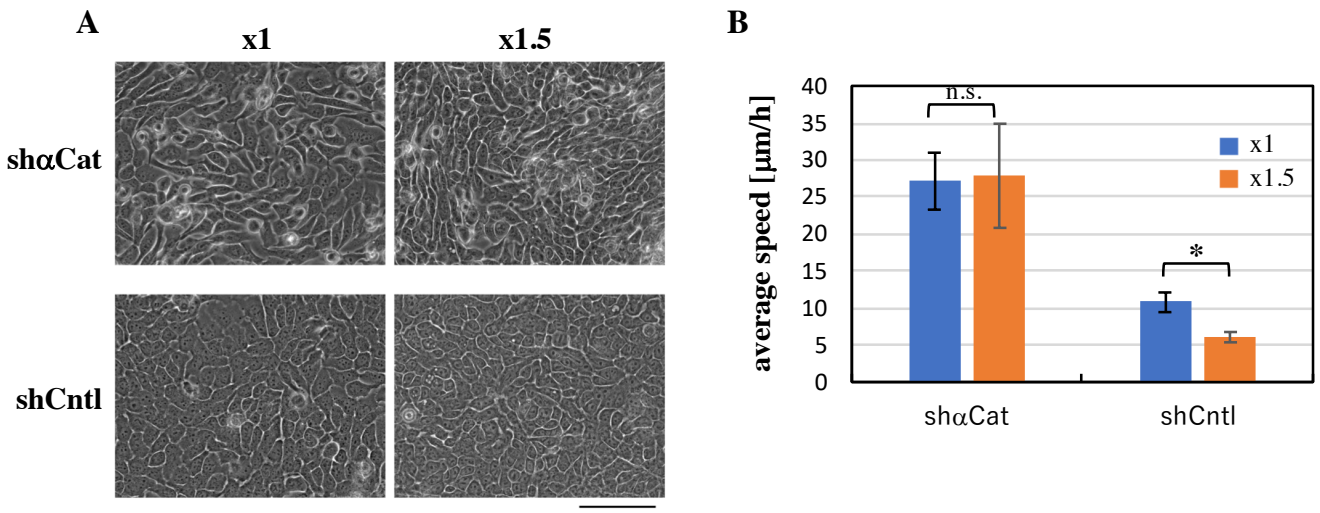

Figure S15. Effect of the cell seeding density on motility of α-catenin-depleted keratinocytes (Related to Figure 4). (A) Phase contrast images of HaCaT cells expressing shRNA against α-catenin (shαCat) or non-targeting shRNA (shCntl) that were seeded at different densities. Images at 20 h after seeding cells are shown. The numbers of seeded cells were 20 x 10^5 cells for "x1" and 30 x 10^5 cells for "x1.5". Scale bar: 100 μm. (B) Average speeds in α-catenin shRNA- or non-targeting shRNA-expressing keratinocyte sheets at 20 h after seeding cells. The numbers of seeded cells were 20 x 10^5 cells for "x1" and 30 x 10^5 cells for "x1.5". Each bar represents mean ± SD (n = 3). *$P < 0.05$; n.s., no significant difference (Student's two-tailed, unpaired *t*-test).

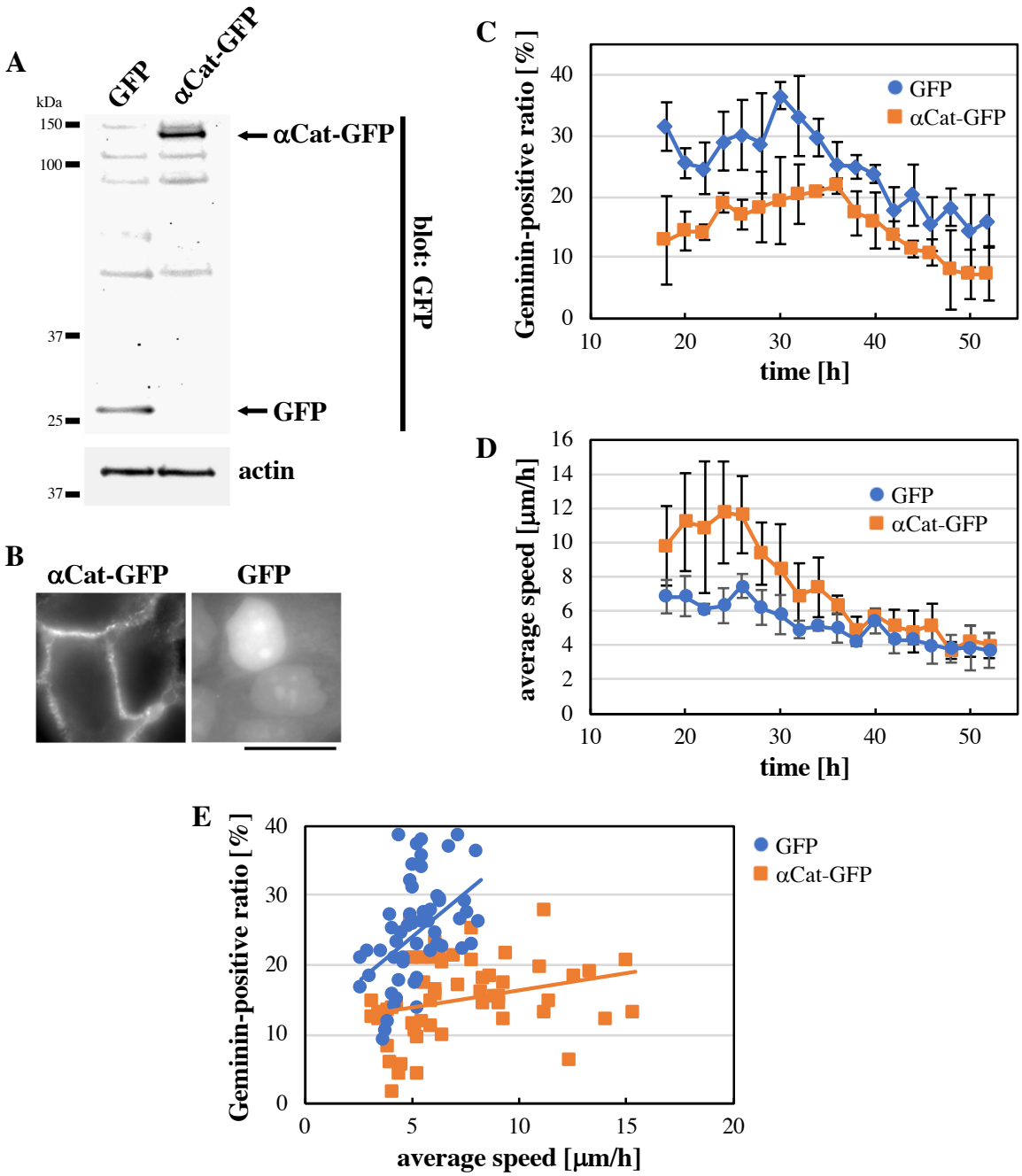

Figure S16. Effect of α-catenin overexpression on cell cycle progression and cell motility in keratinocyte sheets (Related to Figure 4). (A) Immunoblot analyses of expression of α-catenin-GFP (αCat-GFP) and GFP in HaCaT cells. (B) Fluorescence images of α-catenin-GFP (αCat-GFP) and GFP expressed in keratinocyte sheets. Images at 30 h after seeding cells are shown. Scale bar: 20 μm. (C and D) Time-dependent changes in the ratio of Geminin-positive cells (C) and the average speed (D) in keratinocyte sheets expressing α-catenin-GFP (αCat-GFP) or GFP after seeding cells. Each data point represents mean ± SD. n = 3 (> 100 cells at each time point in each experiment in (C)). (E) The ratio of Geminin-positive cells was plotted against the average speed in α-catenin-GFP (αCat-GFP)- or GFP-expressing keratinocyte sheets at each time point throughout observation. Data from three independent experiments were combined for each cell type. Regression lines of linear fitting are shown for both cell types.

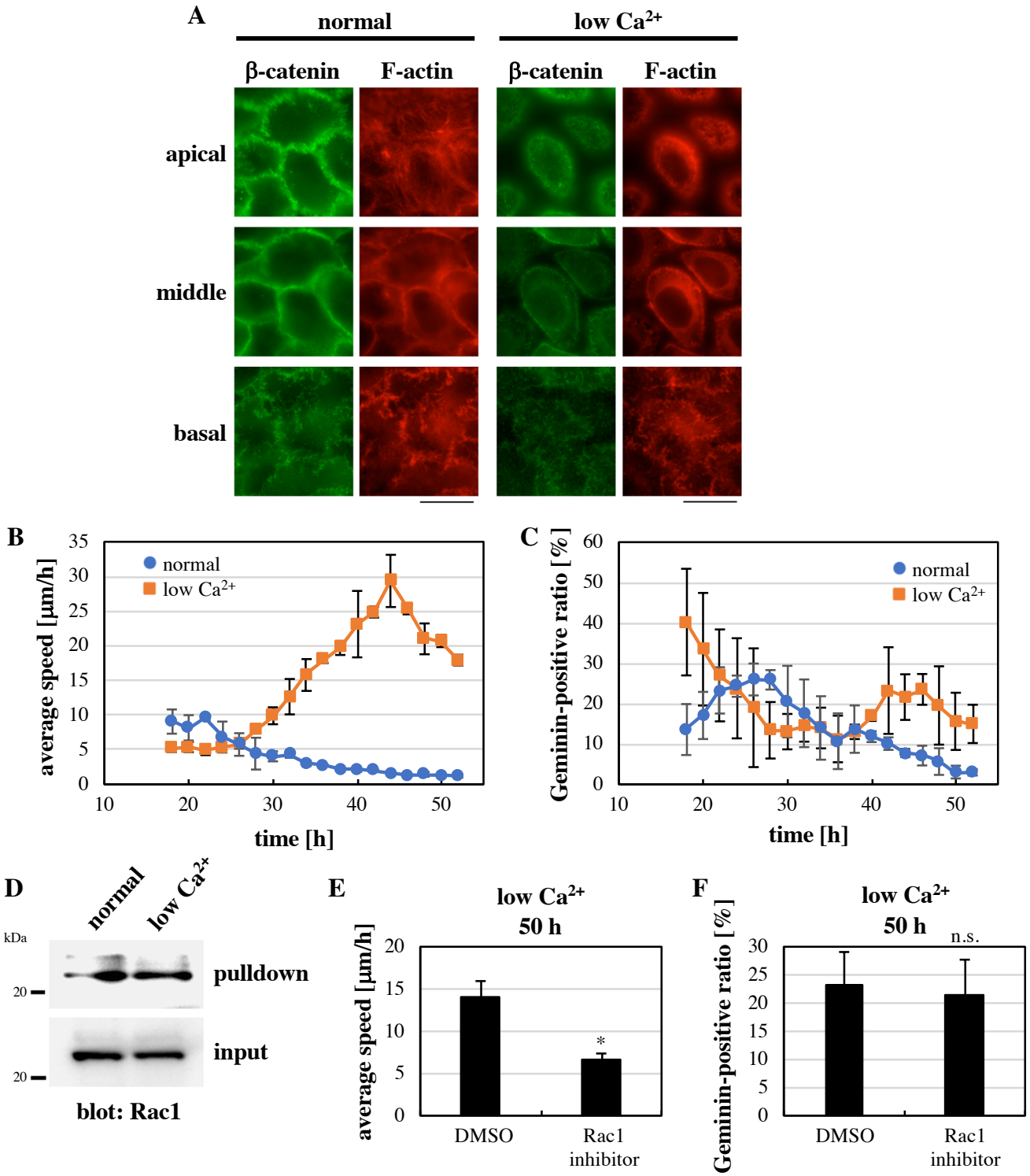

Figure S17. Effect of extracellular Ca^{2+} depletion on cell cycle progression and cell motility in keratinocyte sheets (Related to Figures 4 and 5). (A) Fluorescence images of β-catenin and F-actin at different focal planes of keratinocyte sheets at 50 h after seeding cells in the normal or low Ca^{2+} medium. Scale bars: 20 μm. (B and C) Time-dependent changes in the average speed (B) and the ratio of Geminin-positive cells (C) in keratinocyte sheets after seeding cells in the normal or low Ca^{2+} medium. (D) The Pak1-PBD-based pulldown assay for active Rac1. Lysates of keratinocyte sheets grown for 50 h after seeding cells in the normal or low Ca^{2+} medium were subjected to the assay. (E and F) The average speed (E) and the ratio of Geminin-positive cells (F) in keratinocyte sheets at 50 h after seeding cells in the normal or low Ca^{2+} medium. Each bar represents mean ± SD. n = 3 (> 100 cells in each experiment in (F)). *$P < 0.05$; n.s., no significant difference (Student's two-tailed, unpaired *t*-test).

Transparent Methods

Cell lines

Human HaCaT keratinocytes (Cell Lines Service) and HEK293T cells were maintained in high-glucose Dulbecco's modified Eagle's medium (Nacalai Tesque) supplemented with 10% fetal bovine serum (Thermo Fisher Scientific).

HaCaT cells expressing the Geminin-based Fucci fluorescent cell cycle probe, H2B-GFP, mEGFP-Rac1, mEGFP, or shRNA against α-catenin and/or non-targeting shRNA were generated using the retrovirus system. The retroviral vectors for expression of mEGFP-Rac1 and mEGFP were constructed by subcloning DNA sequences of human Rac1 (provided by Kozo Kaibuchi, Nagoya University, Japan) and/or mEGFP into the pMXs-IRES-Blasticidin plasmid (provided by Toshio Kitamura, University of Tokyo, Japan) (Kitamura et al., 2003). The pRetroX-SG2M-Red (Takara Bio), pMXs-IRES-Blasticidin-mEGFP-Rac1, pMXs-IRES-Blasticidin-mEGFP or pBabe.puro-H2B-GFP (provided by Keiko Kawauchi, Konan University, Japan) plasmid, or the pSUPER.retro.puro or pSUPER.retro.hygro plasmid carrying the sequence of either shRNA against human α-catenin or non-targeting shRNA (Hirata et al., 2017) was co-transfected with the pE-ampho plasmid into HEK293T cells using the GeneJuice transfection reagent (Merck). The HEK293T cell media containing viral particles were collected at 48 h after the transfection, filtered through 0.45-μm filters, and used for infection into HaCaT cells in the presence of 8 μg/ml polybrene (Sigma-Aldrich). Infected HaCaT cells were selected with 4 μg/ml puromycin (Sigma-Aldrich), 1000 μg/ml hygromycin B (Wako Pure Chemical) and/or 7 μg/ml blasticidin S hydrochloride (Wako Pure Chemical).

HaCaT cells expressing RaichuEV-Rac1 were generated using the piggyBac transposase system (Yusa et al., 2009). The expression vectors for RaichuEV-Rac1 (provided by Michiyuki Matsuda, Kyoto University, Japan) and piggyBac transposase (System Biosciences) were co-transfected into HaCaT cells using the GeneJuice transfection reagent. Transfected cells were selected with 7 μg/ml blasticidin S hydrochloride.

αE-catenin-EGFP (provided by Shigenobu Yonemura, Tokushima University, Japan) and EGFP were introduced into HaCaT cells by transfecting the cells with their expression vectors using the GeneJuice transfection reagent. Transfected cells were selected with 800 μg/ml G-418 (Sigma-Aldrich).

F-tractin-EGFP (Johnson and Schell, 2009) was introduced into HaCaT cells by transfecting the cells with its expression vector (provided by Michael J. Schell, Uniformed Services University, USA) using the GeneJuice transfection reagent.

Low Ca^{2+} medium

Ca^{2+}-free, high-glucose Dulbecco's modified Eagle's medium (Nacalai Tesque) was supplemented with 0.3 mM EGTA, 584 mg/l L-glutamine, 110 mg/l sodium pyruvate, 10% fetal bovine serum (Thermo Fisher Scientific). Given the concentration of Ca^{2+} in FBS to be 3.4 mM (Nagakura et al., 1987), the free Ca^{2+} concentration in the low Ca^{2+} medium was estimated as ~40 μM (calculated using Ca-EGTA Calculator v1.3 (Bers et al., 2010)).

Antibodies and chemicals

The mouse monoclonal antibody against cortactin (05-180) and the rabbit polyclonal antibody against Rac1 (07-1464) were obtained from Merck. The rabbit polyclonal antibody against α-catenin (C2018) and the mouse monoclonal antibody against β-actin (A5441) were from Sigma-Aldrich. The rabbit monoclonal antibody against E-cadherin (3195S) was from Cell Signaling Technology. The rabbit polyclonal antibody against β-catenin (ab6302) was from Abcam. Alexa Fluor 488-goat anti-mouse IgG and Alexa Fluor 488-goat anti-rabbit IgG antibodies, and Alexa Fluor 546-phalloidin were from Thermo Fisher Scientific. Horseradish peroxidase (HRP)-conjugated anti-mouse IgG and anti-ribbit IgG antibodies were from GE Healthcare. The Rac1 inhibitor NSC23766 was from Merck. Dimethyl sulfoxide (DMSO) was from Sigma-Aldrich.

Live cell imaging

HaCaT cells expressing the indicated fluorescent probe were seeded (20×10^5 cells for the "dense" condition and 0.3×10^5 cells for the "sparse" condition, otherwise specified) in the presence or absence of the indicated drug onto a 35-mm glass bottom dish (3910-035, AGC Techno Glass) precoated with 50 μg/ml collagen (Koken). Under the "dense" condition of cell seeding, the surface of the collagen-coated glass bottom dish was fully covered with cells. Just after seeding cells, the dish was placed in an observation chamber of the BioStation IM fluorescence microscope (Nikon) under the 37 °C and 5% CO_2 humidified atmosphere. Fluorescence and phase contrast images were captured at 30-min

(for imaging of F-tractin-EGFP, RaichuEV-Rac1 or H2B-GFP) or 10-min (for other cases) intervals. For RaichuEV-Rac1 imaging, the following filters and dichroic mirrors obtained from Nikon were used; the excitation filter FF02-438/24-25, the dichroic mirror FF458-Di02-25x36, and the emission filters FF01-542/27-25 (for FRET) and FF01-483/32-25 (for CFP).

EdU incorporation and immunofluorescence

For the EdU incorporation assay, HaCaT cells grown for the indicated duration after seeding cells in the presence or absence of the indicated drug were incubated for 2 h with 10 μM EdU in the presence or absence of the same drug. The cells were then fixed and permeabilized with 4% formaldehyde and 0.5% Triton X-100, respectively, in PBS, and incorporated EdU was visualized with Alexa Fluor 488-azide using the Click-iT technology (Thermo Fisher Scientific). Total nuclei were stained with 5 μg/ml Hoechst 33342 (Thermo Fisher Scientific).

Immunofluorescence staining was conducted as described previously (Hirata et al., 2008). In brief, cells were fixed and permeabilized for 30 min with 4% formaldehyde and 0.2% Triton X-100 in the cytoskeleton stabilizing buffer (137 mM NaCl, 5 mM KCl, 1.1 mM Na_2HPO_4, 0.4 mM KH_2PO_4, 4 mM $NaHCO_3$, 2 mM $MgCl_2$, 5.5 mM glucose, 2 mM EGTA and 5 mM PIPES, pH 6.1), which was followed by blocking with 1% BSA in the cytoskeleton stabilizing buffer for 30 min. The cells were then incubated with the primary antibody for 40 min, washed, and further incubated with the secondary antibody (and fluorescent phalloidin, when indicated) for 40 min.

Fluorescence images of fixed cells were obtained using an epi-fluorescence inverted microscope (ECLIPSE TE2000-U, Nikon) equipped with an air (NA 0.30, 10 ×; Plan Fluor, Nikon) or an oil immersion (NA 1.45, 100 ×; Plan Apo TIRF, Nikon) objective and a complementary metal oxide semiconductor camera (ORCA-Flash4.0 C11440-22CU, Hamamatsu Photonics). The Metamorph software (version 7.8, Molecular Devices) was used for image acquisition.

Annexin V staining

HaCaT cells were seeded (20×10^5 cells for "× 1" density and 30×10^5 cells for "× 1.5" density) onto 35-mm glass bottom dishes precoated with 50 μg/ml collagen. After culturing for 40 h, the cells were washed twice with PBS, and stained with FITC-

conjugated Annexin V (30018, Biorium) and Hoechst 33342 for 15 min at room temperature. The stained cells were observed with an epi-fluorescence microscope.

Image analyses

All image analyses were conducted using the public domain software ImageJ (version 1.45f).

The number of total cells was obtained by manually counting nuclei in either phase contrast, H2B-GFP or Hoechst 33342 images. Cells with nuclear Fucci fluorescence signal above the background intensity level were counted as Geminin-positive cells.

The velocity vector map in a confluent keratinocyte sheet was obtained by the PIV analysis (vector spacing of 16 pixels by 16 pixels) using the ImageJ plugin PIV (Tseng et al., 2012). Two consecutive frames (corresponding to 10-min time difference) of phase contrast time lapse images were used for each PIV calculation. The average speed in a velocity vector map was calculated by averaging the magnitude of velocity vectors in the map. Aberrantly large velocity vectors sometimes appeared in the PIV results (Figure S3A). Such aberrant vectors are likely to be caused by floating particles in the culture medium. The floating particles moved much faster than cells in keratinocyte sheets, and the large displacement of the particles during a single frame interval (i.e., 10 min) caused local errors in cross-correlation calculation between the frames, leading to appearance of 'spurious vectors' in PIV (Figure S3B). Importantly, the spurious vectors are minor among the calculated vectors (1680 vectors total) in a single PIV field, and appearance of spurious vectors did not affect dominantly the value of average speed in the field. For example, the average speed in Figure S3A was 2.67 μm/h with spurious vectors, and 2.57 μm/h after removing the spurious vectors.

Collectiveness of cell movement in a keratinocyte sheet was evaluated, as follows. The velocity vector map in a keratinocyte sheet at 20-h time point was obtained by the PIV analysis. Along a horizontal line (with a constant y value) in the map, spatial autocorrelation coefficients of velocity vector angles were calculated for different Δx values using the Real Statistics Resource Pack software (Release 6.6.1). The autocorrelation coefficients along all horizontal lines available in the map (35 lines) were averaged for each Δx value, and the correlogram against Δx was created using the averaged autocorrelation coefficients (Figure S12B). The correlogram was fitted with the equation,

$$A(\Delta x) = c \times \left(e^{-d \cdot \Delta x} - 1\right) + 1, \quad [1]$$

where $A(\Delta x)$ is the averaged autocorrelation coefficient at Δx, and c and d are fitting parameters (Figure S12B). The larger the decay constant d is, the shorter the correlation length of spatial distribution of velocity vector angles is, and, therefore, the less collective the cell movement in a keratinocyte sheet is.

The velocity of single cells under the sparse condition was measured by tracking the center of mass of nucleoli for each cell. The region of each nucleolus was determined by setting a threshold level in a phase contrast image. Time frames in which the cell was at the mitosis or cytokinesis stage were excluded from the analysis.

To analyze correlation between cell cycle progression and cell movement in a keratinocyte sheet, the Geminin-positive cells/total cells ratio was plotted against the average speed in the sheet at each time point throughout the observation period. The plots for three keratinocyte sheets were combined together, and the correlation coefficient and the regression line of the combined plots were calculated.

Cortactin-positive lamellipodia regions in an anti-cortactin immunofluorescence image were defined, as follows (Figure S9). After rolling ball subtraction (with the ball radius of 15 pixels) of the background staining, the fluorescence image of cortactin was subjected to median filtering (with the 10-pixel radius) to remove spotty signals outside wavy lamellipodia. In the resultant image, pixels in which the fluorescence intensity was above the threshold level were determined as lamellipodia regions.

Time-dependent changes in the membrane protrusion activity of cells were analyzed using time lapse images of F-tractin-EGFP-expressing cells. After rolling ball subtraction (with the ball radius of 150 pixels) of the background intensity, the region of a cell in which the fluorescence intensity was above a threshold level was determined in each frame. By comparing the cell region in one frame with that in the immediately preceding frame, extended regions of the cell during the time interval (30 min) were identified.

The cell division tree analysis was conducted, as follows. Cells in a phase contrast image at 20 h after seeding cells were randomly chosen as “founders”, and they and their offspring were manually traced until 52 h after the seeding. Cells that escaped from the field of view during the trace were excluded from the analysis. Time points of division of founder cells and their offspring were recorded to construct cell division trees for individual founders. The number of offspring cells derived from each founder cell was

counted at 52 h after seeding cells. If a certain founder cell does not divide until 52 h after the seeding, the number of its offspring becomes one.

Pulldown assay

Specified types of HaCeT cells were seeded (16×10^6 cells for the "dense" condition and 2.4×10^5 cells for the "sparse" condition) onto collagen-coated 10-cm dishes in either normal DMEM or the low Ca^{2+} medium in the presence or absence of the indicated drug, and were grown for the indicated time period. After washing cells with cold PBS, the PAK1-PBD-based pulldown assay for active Rac1 was conducted using the Rac1 activation magnetic beads pulldown assay kit (17-10393, Merck). In brief, the cells were lysed with the Mg^{2+} lysis/wash buffer (MLB) that contained the protease inhibitor cocktail (Cytoskeleton), and centrifuged at 14,000 g for 5 min. The supernatants were used as the cell lysates for further procedures. The cell lysates were incubated with PAK1-PBD-coupled magnetic beads for 45 min at 4 ºC. The beads were washed three times with MLB, and, then, the precipitated proteins were eluted with 2 × lithium dodecyl sulfate sample buffer (Thermo Fisher Scientific) containing 2.5% β-mercaptoethanol (Sigma-Aldrich). The pulldown samples were subjected to the immunoblot analysis for Rac1.

Immunoblot

Cells were lysed with 2 × lithium dodecyl sulfate sample buffer containing 2.5% β-mercaptoethanol. The lysate was resolved by SDS-PAGE (4-12% Bis-Tris gel; Thermo Fisher Scientific), transferred onto the polyvinylidene fluoride membrane (Merck), and probed with primary and HRP-conjugated secondary antibodies. Imuno-reactive bands were detected with Chemi-Lumi One Super (Nacalai Tesque).

Supplemental References

Bers, D.M., Patton, C.W., and Nuccitelli, R. (2010). A practical guide to the preparation of Ca^{2+} buffers. Methods Cell Biol. *99,* 1-26.

Hirata, H., Samsonov, M., and Sokabe, M. (2017). Actomyosin contractility provokes contact inhibition in E-cadherin-ligated keratinocytes. Sci. Rep. *7,* 46326.

Hirata, H., Tatsumi, H., and Sokabe, M. (2008). Mechanical forces facilitate actin polymerization at focal adhesions in a zyxin-dependent manner. J. Cell Sci. *121,* 2795-2804.

Johnson, H.W., and Schell, M.J. (2009). Neuronal IP_3 3-kinase is an F-actin-bundling protein: role in dendritic targeting and regulation of spine morphology. Mol. Biol. Cell *20,* 5166-5180.

Kitamura, T., Koshino, Y., Shibata, F., Oki, T., Nakajima, H., Nosaka, T., and Kumagai, H. (2003). Retrovirus-mediated gene transfer and expression cloning: powerful tools in functional genomics. Exp. Hematol. *31,* 1007-1014.

Nagakura, K., Ueno, M., Brookins, J., Beckman, B.S., and Fisher, J.X. (1987). Effects of low calcium levels on erythropoietin production by human renal carcinoma cells in culture. Am. J. Physiol. *253,* C797-C801.

Tseng, Q., Duchemin-Pelletier, E., Deshiere, A., Balland, M., Guillow, H., Filhol, O., and Théry, M. (2012). Spatial organization of the extracellular matrix regulates cell-cell junction positioning. Proc. Natl. Acad. Sci. U.S.A. *109,* 1506-1511.

Yusa, K., Rad, R., Takeda, J., and Bradley, A. (2009). Generation of transgene-free induced pluripotent mouse stem cells by the piggyBac transposon. Nat. Methods *6,* 363-369.